INVESTIGATION OF LONGITUDINAL SHEAR STRENGTH IN CONCRETE SLABS WITH PROFILED STEEL DECKING

Raushan KAZAKPAYEVA

T.C.
BURSA ULUDAĞ UNIVERSITY
GRADUATE SCHOOL OF NATURAL AND APPLIED SCIENCES

INVESTIGATION OF LONGITUDINAL SHEAR STRENGTH IN CONCRETE SLABS WITH PROFILED STEEL DECKING

Raushan KAZAKPAYEVA

Assoc. Prof. Hakan T. TÜRKER
(Supervisor)

MSc THESIS
DEPARTMENT OF CIVIL ENGINEERING

BURSA – 2021

ÖZET

Yüksek Lisans

ÇELİK SAC VE BETON KOMPOZİT DÖŞEMELERDE BOYUNA KAYMA DAYANIMININ İRDELENMESİ

Raushan KAZAKPAYEVA

Bursa Uludağ Üniversitesi
Fen Bilimleri Enstitüsü
İnşaat Mühendisliği Anabilim Dalı

Danışman: Doç. Dr. Hakan T. TÜRKER

Çelik sac ve beton kompozit döşemeler; çelik yapılarda yaygın kullanılan döşeme tasıyıcı sistemidir. Dünyadaki çelik - beton kompozit yapılarda yüksek gerilme ve esneklik özelliğine sahip çelik ile, yüksek basınç mukavemeti ve korozyon direncine sahip betonun çeşitli kombinasyonları kullanılmakta ve uygulanmaktadır. Kompozit döşemelerin uygulama kolaylığı, yangına karşı iyi performansı, kalıp gerektirmemesi, yüksek eğilme kapasitesi gibi birçok avantajlı yönleri vardır. Ancak kompozit döşemelerin mukavemetini hesaplamak için analitik formüller yoktur. Bu yüzden bu çalışma en gerçekçi davranışı yansıtabilecek sayısal bir model simüle etmeyi amaçlamıştır. Bu amaca ulaşmak için çelik sac ve beton arasındaki etkileşimin modellenmesine en çok dikkat edildi. Çünkü bu tip döşeme tasarımında dikkate alınması gereken en kritik sınır değerlerden biri boyuna kesme dayanımıdır. Etkileşim iki aşamaya bölünmüştür: ilk aşama bir kimyasal bağ çalışmasıydı, ikinci aşama mekanik ve sürtünme faktörlerinin etkisi olduğu aşamaydı. İlk kaymada kesme mukavemeti ve mekanik kilitleme gibi en önemli iki faktör varsayılmıştır. VEM modelinin kullanılması lifli döşemeler için ilk kaymanın hesaplanmasını ve lifli kompozit döşemelerin etkileşimin modellenmesini sağlamıştır. Sonuç olarak lifli döşemeler lifsiz döşemelere göre toplam dayanım ve ilk kaymadaki yükte önemli ve tutarlı gelişmeler gösterdi. Çelik-beton ara yüzeyinde çelik liflerin sağladığı kesme bağı davranışındaki iyileşme nicelleştirilmiştir.Son olarak daha önce yapılmış olan kompozit döşeme deney sonuçları sonlu elemanlar modellerinde elde edilen sonuçlarla kıyaslanmıştır.

Anahtar Kelimeler: Kompozit döşeme, çelik sac, boyuna kayma dayanımı, sonlu elemanlar yöntemi, çelik lifler

2021, xii + 71 sayfa.

ABSTRACT

MSc Thesis

INVESTIGATION OF LONGITUDINAL SHEAR STRENGTH IN CONCRETE SLABS WITH PROFILED STEEL DECKING

Raushan KAZAKPAYEVA

Bursa Uludağ University
Graduate School of Natural and Applied Sciences
Department of Civil Engineering

Supervisor: Assoc. Prof. Hakan T. TÜRKER

Composite slabs with profiled steel decking are widely used in floor carrier systems of steel structures. Various combinations of steel with high tensile and ductility properties and concrete with high compressive strength and corrosion resistance are used and applied worldwide in steel and concrete composite structures. Composite slabs have many advantages, such as ease of application, good performance against fire, no mold required, and high-bending capacity. But there are no analytical formulas for calculating the strength of composite slabs. Therefore, this study had the aim to simulate a numerical model which could reflect the most realistic behavior. The most significant attention was given to model the interaction between steel deck and concrete to achieve this aim. Because one of the most critical limit values to be considered in this type of slab design was the longitudinal shear strength. The interaction was seen as two stages, where the first stage was a work of chemical bond, the second stage was the influence of mechanical and frictional factors. The two most important factors as shear strength in first slip and mechanical interlock were assumed. Using the Variable Engagement Model allowed calculating the first slip for the SFRC slabs and using it in the interaction model of composite slabs. The SFRC slabs showed significant and consistent improvements in the overall strength and the load at first slip compared to the plain concrete slabs. The improvement in the shear-bond behavior afforded by the steel fibers at the steel-concrete interface has been quantified. In the end, composite slabs test results that were made before were compared with the results obtained in numerical models.

Key words: Composite slab, steel decking, longitudinal shear bond strength, finite element method, steel fibers.

2021, xii + 71 sayfa.

ACKNOWLEDGEMENT

The author wishes to express her gratitude and appreciation to many people for their support and encouragement to complete this research. In addition, I would like to thank my supervisor, Assoc. Prof. Hakan T. TÜRKER for providing guidance and feedback throughout this thesis, also for encouragement and patience.

From the bottom of my heart, I would like to say a big thank you to Prof. Babür DELİKTAŞ for his invaluable advice, continuous support, and patience during my Master's study. His immense knowledge and great experience have encouraged me in my academic research and daily life.

Further, I would like to thank to all my friends and Master candidates with whom I shared this priceless experience and the challenges, both the highs and the lows. I am very grateful for their company and friendship throughout the time of Master. Their kind help and support have made my study and life at Bursa Uludağ University a wonderful time. I would like to say a special thank you to Ibrahim Hamid, Aiman Tariq and Mohamed Sheriff Jalloh for their overwhelming support.

Finally, I must express my very profound gratitude to my mother for her endless support and continuous encouragement throughout my years of study and through the process of researching and writing this thesis. You have always stayed behind me, and this was no exception. Mom, thank you for all of your love and for always reminding me of the end goal.

Raushan KAZAKPAYEVA
11/08/2021

CONTENTS

Page

ÖZET i
ABSTRACT ii
PREFACE AND/OR ACKNOWLEGDEMENT iii
SYMBOLS and ABBREVIATIONS v
FIGURES vi
TABLES viii
1. INTRODUCTION 1
1.1 Overview of steel-concrete composite slabs 1
1.2 The longitudinal shear strength 2
1.3 Research Aim and Scope 3
1.4 Thesis Contents 3
2. THEORETICAL BASICS AND LITERATURE REVIEW 5
2.1 Deck Types 5
2.2 Composite Deck Construction 7
2.3 Failure modes 9
2.4 Experimental studies of the bond between steel deck and concrete 10
2.5 Shear bond study by numerical methods 12
2.6 Investigations the effect of steel fiber on the shear bond strength between elements of composite slabs 17
3. MATERIALS and METHODS 20
3.1 General Description of Finite Element Method 20
3.2 Finite Element Model 20
3.2.1 Modeling and Model Geometry 22
3.2.2 Material Properties 25
3.2.3 Step 33
3.2.4 Incremental loading 34
3.2.5. Detailed description of all interactions 36
4. RESULTS AND DISCUSSIONS 49
4.1. Mesh Convergence 49
4.2. Calibration and comparison of numerical model with the experimental results 52
4.2.1. Numerical results for the long composite slabs with plain concrete CS-1, CS-2, CS-3 52
4.2.2. Numerical results for the short composite slabs CS-5, CS-6. 55
4.2.3. Numerical result for the long composite slab CS-7 with 0.5% steel fiber 58
4.2.4. Numerical result for the long composite slab CS-8 with 1% steel fiber 60
4.2.5. Numerical result for the long composite slab CS-9 with 1.5% steel fiber 62
4.3. Comparison of the results obtained from laboratory tests, m-k method, partial connection method and numerical model. 65
5. CONCLUSION 67
REFERENCES 68
RESUME 71

SYMBOLS and ABBREVIATIONS

Symbols	Definition
A_c	cross area of the concrete block
A_p	cross area of the steel deck
b	width of slab
b_{em}	effective width of the slab
d_p	effective depth of the slab
t	thickness of the steel deck
L	span length
L_0	cantilever length of the composite slab near the support
L_s	shear span length
h	depth of the slab
E_c	concrete Young's modulus
E_s	steel Young's modulus
δ	midspan deflection
f_{yd}	yield strength of the steel deck
I	moment of the inertia of the steel deck
k	ordinate intercept of shear-bond line, m-k method
m	slope of experimental shear-bond line, m-k method
P_{max}	maximum load
s	longitudinal relative slip
s_1	longitudinal relative slip, first-slip point
s_2	iterated longitudinal relative slip, maximum load point
s_3	longitudinal relative slip, post-crushing point
V_t	vertical shear force
e_c	concrete deformation
e_s	steel deformation
η	connection degree of the slab
τ	longitudinal shear-bond stress
τ_u	ultimate shear stress
τ_1	ultimate shear stress, first-slip point
τ_2	ultimate shear stress, maximum load point
τ_3	ultimate shear stress, post-crushing point
μ	steel-concrete friction coefficient

Abbreviation	Definition
FEM	finite element method
LCCS	lightweight aggregate concrete and closed profiled steel sheeting
LWAC	lightweight aggregate concrete
NWC	normal weight concrete
FE	Finite Element

FIGURES

Page

Figure 1.1. Composite slab with profiled steel deck 1
Figure 1.2. A typical example of composite slab construction, showing the deck placing on a steel frame. 2
Figure 2.1. Trapezoidal and re-entrant types of steel decks 5
Figure 2.2. Connection types between steel deck and concrete 6
Figure 2.3. Patterns of Embossment in Composite Deck 7
Figure 2.4. Installation of composite slabs 9
Figure 2.5. Shear stress versus inverted slenderness in a composite slab in a four-point bending test showing three different failure modes. (a) Elevation and section of a slab specimen in four-point bending test and (b) nominal shear stress versus inverted slenderness of the slab. 10
Figure 2.6. Typical shear resistance versus slip behavior 11
Figure 2.7. τ-s shear-bond law considered for the connector elements. 16
Figure 2.8. Stress versus crack opening/sliding displacement for a fiber reinforced cementitious composite. 18
Figure 3.1. The supporting and loading system of experiment tests: a) long slab; b)short slab. 21
Figure 3.2. The steel deck parameters 22
Figure 3.3. Six independent parts 23
Figure 3.4. Model assemblage 23
Figure 3.5. Type of elements 24
Figure 3.6. A quarter of the composite slab 24
Figure 3.7. Elastic plactic damage law 25
Figure 3.8. Response of concrete to a uniaxial loading condition: (a) Compression, (b) Tension. 26
Figure 3.9. Compression curves of concrete B43: (a) Engineering stress versus engineering strain, (b) True stress versus true strain. 27
Figure 3.10. Tension curves of concrete B43: (a) Engineering stress versus engineering strain, (b) True stress versus true strain. 28
Figure 3.11. Compression curves of concrete B43: (a) True stress versus plastic strain, (b) Damage parameter versus plastic strain. 29
Figure 3.12. Tension curves of concrete B43: (a) True stress versus cracking strain, (b) Damage parameter versus cracking strain. 30
Figure 3.13. Steel parameters used in Abaqus. 32
Figure 3.14. Smooth amplitude (displacement) curve to control the applied displacement. 34
Figure 3.15. Interaction between concrete slab and steel deck 36
Figure 3.16. Typical shear resistance versus slip behavior of composite slab. 37
Figure 3.17. General Contact interaction 38
Figure 3.18. Typical traction-separation response. 39
Figure 3.19. Different types of failure modes 40
Figure 3.20. Cohesive Behavior defined between the steel deck and plain concrete. 41
Figure 3.21. Slip regions for the basic Coulomb friction model. 42
Figure 3.22. Frictional Behavior 42
Figure 3.23. Normal Behavior 43

Figure 3.24. Damage initiation of composite slab with plain concrete. 44
Figure 3.25. Typical stress versus strain and stress versus crack opening displacement for the steel-fiber reinforced concrete in tension.....46
Figure 4.1. Different mesh densities 50
Figure 4.2. Partitions..... 51
Figure 4.3. Curves of mesh convergence result: (a) force versus the number of elements; (b) displacement versus the number of elements..... 51
Figure 4.4. Numerical and experimental results of load versus mid-span deflection of slabs CS-1, CS-2, CS-3.....53
Figure 4.5. Numerical and experimental results of load versus displacement obtained underneath of the loading point of slabs CS-1, CS-2, CS-3.....54
Figure 4.6. Numerical and experimental results of load versus end-slip of long slabs CS-1, CS-2, CS-3.....55
Figure 4.7. Numerical and experimental results of load versus mid-span deflection of short slabs CS-5, CS-6.....56
Figure 4.8. Numerical and experimental results of load versus displacement underneath of the loading point of short slabs CS-5, CS-6.....57
Figure 4.9. Numerical and experimental results of load versus end-slip of short slabs CS-5, CS-6.....58
Figure 4.10. Numerical and experimental result of load versus mid-span deflection of long slab CS-7 and numerical model (0.5% steel-fiber).....59
Figure 4.11. Numerical and experimental result of load versus displacement obtained underneath of the loading point of long slab CS-7……60
Figure 4.12. Numerical and experimental results of load versus end-slip of long slab CS-7 with 0.5% steel fiber.....61
Figure 4.13. Numerical and experimental result of load versus mid-span displacement of long slab CS-8 (1% steel-fiber).....61
Figure 4.14. Numerical and experimental result of load versus displacement obtained underneath of the loading point of long slab CS-8 (1% steel-fiber) ……62
Figure 4.15. Numerical and experimental result of load versus end-slip of long slab CS-8 (1% steel-fiber).....63
Figure 4.16. Numerical and experimental result of load versus mid-span displacement of long slab CS-9 (1.5% steel-fiber).....64
Figure 4.17. Numerical and experimental result of load versus displacement obtained underneath of the loading point of long slab CS-9 (1.5% steel-fiber). ……...65
Figure 4.18. Numerical and experimental results of load versus end-slip of long slab CS-9 (1.5% steel-fiber).....65

TABLES

Table 3.1. Properties of composite slabs 22
Table 3.2. Parameters of steel: (a) engineering data; (b) true data. 32
Table 3.3. τ_{slip} for steel fiber composite slab when using 35 mm hooked-end type with an aspect ratio of 50 and f_{ct}=2.5MPa. 48
Table 4.1. The comparison of the results obtained from laboratory tests, m-k method, partial connection method and numerical model. 65

1. INTRODUCTION

1.1 Overview of steel-concrete composite slabs

Composite slabs are economically viable and efficient types of slabs for different kinds of construction. Composite slabs were created in the late 1930s to replace the traditional reinforced concrete slabs, and in a short period, they became widely used in the world. A combination of the structural properties of concrete with cold-formed steel decking gives a structural slab system named composite slab. A composite slab consists of monolithic concrete, reinforcement, and cold-formed steel decking, which has a thickness usually between 0.75 and 1.25 mm (Figure 1.1). This structure acts like a reinforced concrete structural element when the concrete hardens. Steel deck has two significant meanings: permanent formwork during concreting and tension reinforcement after the concrete has hardened. Subsequently, horizontal shear forces can be transmitted at the junction of steel and concrete, where the connection between the profiled steel deck and the top concrete cover is located.

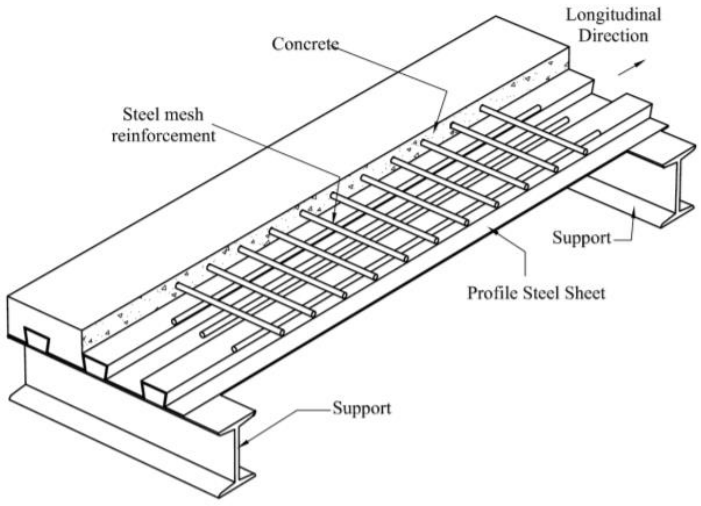


Figure 1.1. Composite slab with profiled steel deck

The structure of a composite slab is a one-sided overlap of covering structures. The slabs are usually laid on the secondary floor beams that are installed on the main beams. The main beams are laid between the spans of the columns. This structural loading system allows the creation of rectangular grids with large one-sided spans. (Structural Steel

Eurocodes 2001.) A typical example of the construction of a composite slab is shown in Figure 1.2.



Figure 1.2. A typical example of composite slab construction, showing the deck placing on a steel frame.

Composite systems are interesting for steel-framed high-rise buildings because they decrease the dead-load and the time spent on construction. Due to the massive use of fast-track construction in the late 1980s, interest in metal structures, particularly composite slabs, increased. Currently, composite slabs are combined with concrete, pre-stressed concrete, and timber structures and can be used in office and administrative buildings, residential and public buildings, parking lots, industrial buildings, and renovation plans (Veljkovic 1996).

1.2 The longitudinal shear strength

In practice, in most cases, the horizontal shear bond between concrete and steel deck influences the strength and behavior of a composite slab. Consequently, longitudinal shear failure is the most common mode of failure. When the composite slab bends, longitudinal shear forces between the steel deck and the concrete generate longitudinal sliding between the two surfaces (Cifuentes and Medina 2013). This relationship between the steel deck and the hardened concrete is due to the transfer of horizontal shear stresses

at the interface between the steel deck and the concrete slab (Ferrer, Marimon and Crisinel 2006, Johnson 2004).

The longitudinal shear strength of a certain type of steel deck is usually estimated by full-scale load experiments and two methods from Eurocode 4. m-k method and Partial Shear method are names of these two methods from Eurocode 4. There are no analytical formulas for calculating the longitudinal shear strength since many parameters affect it. So even the standards contain empirical formulas.

1.3 Research Aim and Scope

As mentioned above, there are no analytical formulas for calculating the strength of composite slabs. Therefore, to confirm the empirical formulas, all firms producing different steel decks must carry out full-scale load experiments for each type of deck. It requires more material costs, time, and labor, so successful simulation can reduce this and get results close to reality without too many tests.

The aim of this thesis is to model composite slabs with the finite element method, for which longitudinal shear capacity tests were carried out according to Eurocode 4 by Başsürücü (2013). Finite Element modeling was done using the ABAQUS/Explicit program. The results from the simulation and the experiments were compared and evaluated.

1.4 Thesis Contents

The preceding sections outlined an Overview of steel-concrete composite slabs, deck types, composite deck construction, failure modes, and research aim and scope. This section presents the content of the thesis. This thesis is divided into five chapters.

Chapter two provides a comprehensive demonstration of the experimental and analytical studies on composite slabs investigated by other researchers and the theoretical basis.

Chapter three presents the general description of the finite element method. A numerical model was created to understand how friction and contact are modeled in the Abacus program. Furthermore, the constitutive law of materials used in the model was presented. In addition, a comprehensive discussion of the interaction part is provided. The modeling method of steel-fiber composite slabs is considered too.

Chapter four consists of a full-scale model with the same parameters and material properties as experimental tests. This Chapter includes comparisons of the experiments carried out by Bassürücü (2013) test results and the numerical analysis performed using the finite element method. In addition, results and discussion are discussed in detail.

Finally, in chapter five conclusions and recommendations were provided in detail. In addition, recommendations for future studies have also been added.

2. THEORETICAL BASICS AND LITERATURE REVIEW

This chapter includes theory of composite slabs on longitudinal shear strength and a literature review of related publications. The studies included in this chapter ranged between experimental and numerical studies. Experimental studies were carried out using the methods specified at Eurocode 4, while the numerical studies were conducted using the finite element method. In this study, some methods and recommendations from the previous studies were used. In addition, a review of recent research on numerical modeling of composite slabs, both with or without steel fibers, was investigated.

2.1 Deck Types

Cross-section shapes of cold-formed profiles are manufactured from thin steel strips of grades S280 and S350. To reduce the stress in the steel that appeared during the cold rolling process it is necessary to carry out the annealing process. Thanks to this, the steel strip has increased ductility and higher strength to weight ratio. The yield strength of the steel rises by the cold forming and strain hardening process. In a reinforced section, the yield strength can increase from 10% to 30% through cold forming (Vakil 2017).

Decking profiles usually have a height of 45 to 80 mm and a groove spacing of 150 to 300 mm. Steel strips with a thickness of 0.9 to 1.5 mm are used for cold-rolled profiles. There are two types of steel decks: Trapezoidal and Re-entrant (commonly known as dovetail) as shown in Figure 2.1(a) and Figure 2.1(b) (Nethercot 2003).

Complex interaction between the trapezoidal type of steel deck and concrete occurs due to indentations, embossments, or mechanical interlock. In contrast, for the Re-Entrant profile, frictional interlock promotes this bond (Vakil 2017).



(a) Trapezoidal Profile (b) Re-entrant Profile

Figure 2.1. Trapezoidal and re-entrant types of steel decks (EN 1994-1-1:2005)

A sufficiently strong interaction should be created between the concrete and the deck for making the steel deck more sustainable to vertical separation and longitudinal slip. In most cases, to obtain this interaction, adhesion is not enough. An effective connection can be achieved in the following ways, as shown in Figure 2.2 (a) - Figure 2.2 (d) (EN 1994-1-1:2005).

a) Frictional interlock for Re-entrant profile
b) Mechanical interlock obtained by indentations, embossments, protrusion, holes.
c) End anchorage obtained by welded studs
d) End anchorage obtained by deformation of the ribs

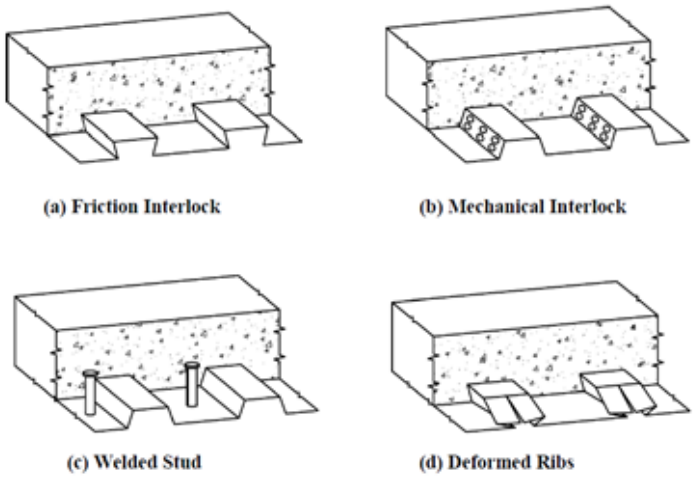


Figure 2.2. Connection types between steel deck and concrete (EN 1994-1-1:2005)

Embossment in Composite Deck

Embossment is one of the most popular types of mechanical interlocks between steel deck and concrete. There are many types of geometry of embossments that can be produced by pressing and rolling. As shown in Figure 2.3, there are reliefs with shapes such as horizontal, sloping, chevrons, stepped, rectangular and circular. The available pressing areas and the quality of the steel sheet of the deck directly affect the location of the embossments. At the same time, the energy demand for pressing is taken into account to determine the height and depth and avoid sheet breakage (Vakil 2017).

Strict inspection and quality control ensure the correct depth of embossment. Inelastic material and poor adjustment or wear on rollers can lead to “unequal” and “absent” depth.

Excessively deep embossment can cause a weakening of the load-bearing capacity of the deck, as well as premature wear. The superficial embossment creates an opportunity for an early loss of interaction in the composite structure immediately after the fabrication stage, which entails safety concerns.

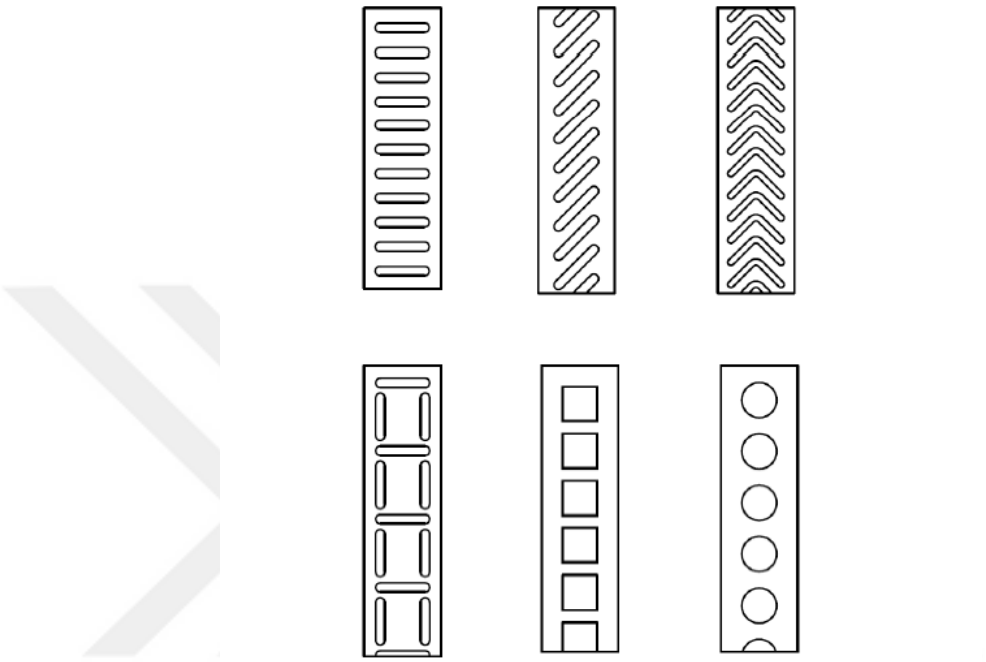


Figure 2.3. Patterns of Embossment in Composite Deck (Vakil 2017)

Typically, the maximum span is determined by the deck's ability to carry loads that occur during construction. Therefore, it is advantageous to use lightweight concrete (wet density 1850–1950 kg/m^3). For decks with superficial embossments, the span is usually around 3–4 m. But for decks with deep embossments, this value is more than 6 m (Nethercot 2003).

2.2 Composite Deck Construction

The construction process of a composite slab is fundamentally different from a conventional reinforced concrete slab. This process consists of several steps, from the installation of the steel deck to the pouring of the concrete.

The sequence of composite slab construction:

1. Installation of Steel Deck.

The steel deck is laid over structural steel or directly attached to a beam at predetermined points during installation. The steel deck connects with the structural steel by welding or powder-powered tools, and then the nail fastener is threaded through the steel deck into the steel beam. Depending on the sizes, materials, and grades available, head stud connectors are used to create a durable bond between the steel beam and the steel deck. Welded wire mesh or reinforcing mesh is installed on the deck to prevent cracking due to temperature and shrinkage (Vakil 2017). The process from laying of the deck to the installation of reinforcement is shown in Figure 2.4 (a) to Figure 2.4 (c).

2. Installation of Concrete.

After installing the deck, concrete is poured over it, usually using the pumping method. In cases with a large deck span, supports should be used to avoid big deflection. An experienced concrete contractor should be involved in the concrete work because concrete must first be laid over the supporting elements and then spread towards the center of the span. Also, the accumulation of concrete in a certain area, usually in the center, should be voided, as this leads to the accumulation of water. During the solidification of the concrete composite bond is formed with the steel deck. The concreting process is described by the photographs shown in Figure 2.4 (d) to Figure 2.4 (f).



Figure 2.4. Installation of composite slabs (Başsürücü 2013)

2.3 Failure modes

Many factors affect the performance of a composite slab such as compressive strength of concrete, location of the load, geometry, and the thickness of the steel deck (Patrick and Bridge 1994).

The design of the composite slab design should take into account the ability to resist the maximum loads at the ultimate state. Figure 2.5 (a) represents a four-point bending test from an elevation view and a cross-section view of a composite slab. This Figure shows three types of existing modes of failure (Gholamhoseini et al. 2014):

1. flexural failure at the peak moment zone (i.e., at section b—b),
2. longitudinal shear failure at zone c—c,
3. vertical shear failure at zone a—a.

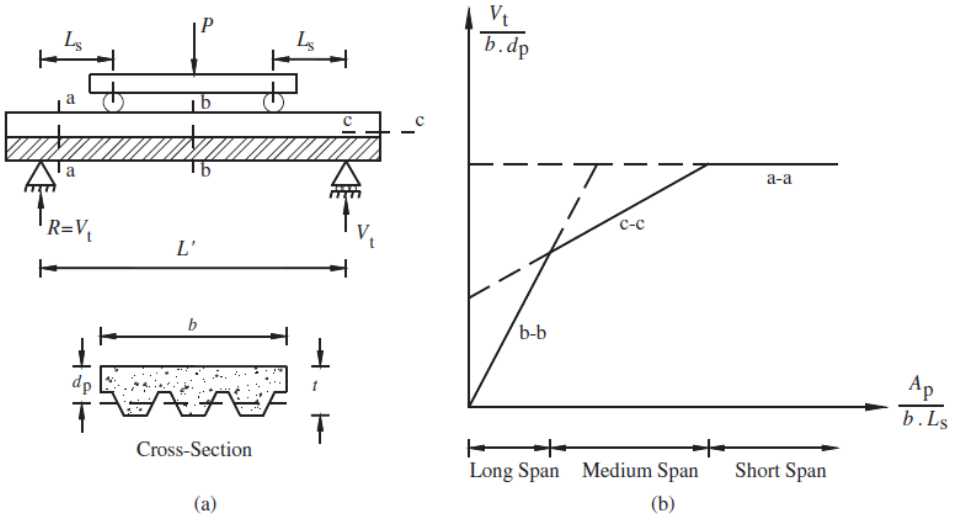


Figure 2.5. Shear stress versus inverted slenderness in a composite slab in a four-point bending test showing three different failure modes. (a) Elevation and section of a slab specimen in a four-point bending test and (b) nominal shear stress versus inverted slenderness of the slab (Gholamhoseini et al. 2014).

Figure 2.5 (b) illustrates how the nominal shear stress value ($V_t/b \cdot d_p$) interacts with the inverted slenderness of the slab ($A_p/b \cdot L_s$). This graph is divided into three parts corresponding to a three-failure pattern. In the first part, when L_s is large flexural failure occurs. In the third part, L_s is small, so vertical shear failure happens. The second part illustrates that the intermediate value of L_s causes longitudinal shear failure (Gholamhoseini et al. 2014).

2.4 Experimental studies of the bond between steel deck and concrete

The main characteristic of composite structures is the ability to transfer forces between components, i.e., the steel deck and concrete in a composite slab (Oehler and Bradford, 1995). Therefore, the load-carrying capacity of composite slabs largely depends on the ability of these two materials to connect and the friction behavior (Schuster and Ling 1980; Tremblay, Roger, et al. 2002; Vainiunas, Valivonis, et al. 2006).

Daniels and Crisinel (1993) were among the first who described this relationship between the steel deck and concrete in more detail. They provided an experimental study where a small-scale pull-out test was carried out to investigate the strength and behavior of the

longitudinal shear between the steel deck and the concrete. The test showed that the pull-out test was acceptable to investigate the shear bond without shear studs because the early push-out test was more desirable for the test specimen with end restraint. The authors attached great importance to the fact that the mechanism of shear transfer occurs due to a chemical bond, mechanical and frictional interactions. It has been observed that the mechanical and frictional interactions are expressions of the same phenomenon but at different magnitudes of geometry irregularities.

In his pull-out test, the authors observed that significant load continued to be carried well after the maximum load had been attained. The maximum load was observed at slips of 1 mm to 4 mm for the embossed decking type.

Figure 2.6 demonstrates the typical behavior of composite slabs under pull-out tests, described in terms of shear resistance versus slip. As a result of the observation, two main distinguishing behaviors were identified. The first behavior is the adhesive bond (chemical bond). The example of brittle fracture well illustrates this. Due to the combination of mechanical interlocking and friction, the second behavior showed ductile behavior up to breaking slip point.

Thereby the characteristics of the second behavior manage the interface resistance, which increases gradually.

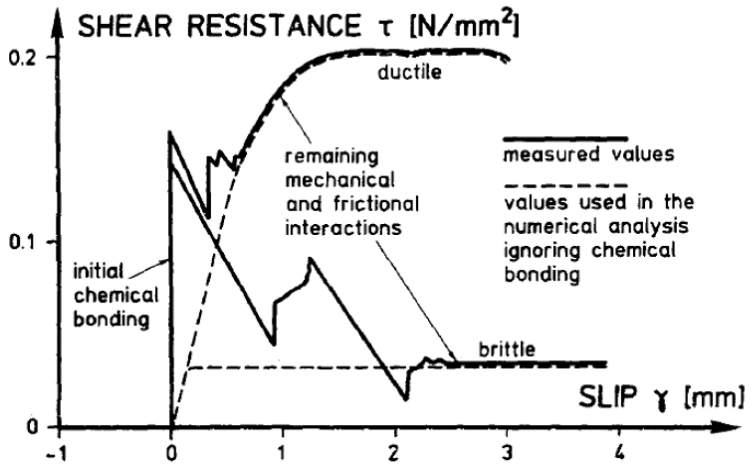


Figure 2.6. Typical shear resistance versus slip behavior (Daniels and Crisinel 1993)

2.5 Shear bond study by numerical methods

Milan Veljkovic (1996) analyzed composite slabs which fail in longitudinal shear and flexural failure. An analytical approach based on FE simulations and data from small-scale tests (detail tests) has been used. A pilot version of DIANA 5.1 (TNO, Delft, The Netherlands) was used to perform the FE analysis. The simulation has paid great attention to such things as friction between the steel deck and concrete, the resistance of mechanical interlocking, and deterioration of mechanical interlocking due to large deformation in the deck. To model the trapezoidal shape of the steel deck, the curved shell element Q20SH was selected. Different uniaxial stress and strain ratios were used for web and flanges. For this, tensile tests were carried out on flat and corrugated sheets. The effect of the cold forming on the properties of sheet material (yield strength and ductility), was not taken into account. The results obtained that the pressed indentations reduce the effective yield strength and Young's modulus to 47% of the initial values for a flat sheet. That is a result of bending deformations of the folds added to the tensile deformation. The concrete deck was designed using the HX24L solid element and interface element Q24IF (the length is 50 mm). As the material properties of concrete, a nonlinear elastic constitutive model is used, which provides the plasticity of concrete under compression.

The crack inducer used in the experiment is modeled with a quadrilateral interface element. A nodal interface element named N4IF was used to reproduce the effect of indentations and the re-entrant portion between the steel deck and concrete. A nonlinear elastic constitutive model helped to recreate longitudinal slip-stress relation, which has been taken from small-scale tests. Also, the coefficient of friction was investigated by tests as 0.6. The author neglected the values of cohesion and dilatancy angle. The advantage of symmetry was used, so only half of the single-span simply-supported slab was designed considering the loading pattern and the supports. Experimental and simulation results showed that the relationship between longitudinal shear and slip, concrete cracking, and deterioration of mechanical interlocking due to large deformation in the deck are of prime importance on the bearing capacity of the composite slab. Ultimately, Veljkovic assumed that about 90% of the shear transmission accounted for the interface element located at the folds of the steel deck. Good results were obtained by

comparing the experimental results with simulation results. Based on simulation results, Veljkovic suggested that another cracking function of concrete did not lead to qualitatively new information about the mechanism of destruction, but it ensured numerical convergence and stability. In this research, the author qualitatively investigated the mechanisms of force transmission from the steel deck to the concrete during sliding. It was discovered that the same mechanism of behavior was demonstrated in both small-scale and full-scale tests. Parameters such as horizontal force, slip relationship, and friction coefficient were sufficient to predict composite slabs' behavior with longitudinal shear failure.

Ferrer, Marimon, et al. (2006) investigated the influence of geometric shape on the bearing capacity of a composite slab using the finite element method. Like other authors in previous works, the authors neglected the adhesive bond and, in their models, only considered friction coefficients from 0.2 to 0.6. To simplify the model, a rigid solid concrete element was used instead of the solid elastic element because concrete has a much higher stiffness than a steel deck. Thus, it was possible to avoid the destruction of concrete in the simulation. They concluded from their numerical models that the slip resistance was linearly dependent on the coefficient of friction. In addition, at the expense of ductility, the relief slope of the steel deck significantly influences the shear strength of the composite slab.

Chen and Shi (2011) have done comparative research between experimental test results of composite slabs with trapezoidal and Re-Entrant profiles of steel deck and numerical study using the software package ANSYS. They were one of the first to use the connector element, which included cohesive and friction behavior and thus described behavior at the interface between concrete and steel deck. As material properties of the connector element, the Coulomb friction model was chosen. The main parameters were taken from the pullout test results carried out by Daniels and Crisinel (1993). The maximum stress on adhesion behavior for the trapezoidal type of deck was taken at 0.06 MPa, while for the Re-Entrant profile, it was 0.08 MPa. The authors believed that the composite slabs collapsed due to longitudinal shear caused by small cracks in the concrete slab leading to delamination and sliding between the steel deck and the concrete. They also stated that

shear stress and slip are unevenly distributed over the entire span. It was also investigated that slip decreases from the end of the slab to the middle of the span, corresponding to a higher shear bond stress in the shear span than the pure bend area.

Shubhangi Attarde (2014, Master's thesis, Toronto) focused on the nonlinear modeling of one-way composite slabs consisting of steel deck and one of two types of concrete (Engineered Cementitious Composites [ECC] and Self-Consolidating Concrete [SCC]). Two FE models were designed based on the results of an experiment of monotonic loading of composite plates in the plane. Two types of contact properties have been selected to describe the relationship between the steel deck and the concrete. The first one was tangential behavior. Tangential behavior is specified to create a friction model that increases the resistance to relative tangential movement of surfaces in an analysis of mechanical contact. For permitting some relative movement of surfaces, the friction formulation area between the contact surfaces was chosen as a "penalty." Directionality was selected as "isotropic," and the friction coefficient used is 0.5. The FE model did not include the slip-rate dependent used in the experimental test because it simplified the analysis. The second contact property was normal behavior defined as "Hard" contact, and the "Default" forced restraint method was chosen to enable the ABAQUS/Explicit analysis. Furthermore, after the steel deck and concrete came in contact with each other, the separation of these two surfaces was excluded. Otherwise, complex behavior would not be observed since there would be no friction. The obtained data of load-deflection, shear bond capacity, and moment resistance are in good agreement with the results of the experiments. Using the finite model, Shubhangi Attarde also conducted complex parametric studies to analyze the influence of parameters such as the interaction between the steel deck and concrete, properties of materials, mesh size, a span of slabs, and dilation angle.

Gholamhoseini et al. (2014) presented the results of short-term testing of eight composite slabs. For constructing these slabs, two re-entrant profiles (RF55, KF57) and two trapezoidal profiles (KF40, KF70) were used. These types of steel decks are the most widely used in Australia. The composite slabs did not conclude reinforcing steel. Full-scale samples of simple support slabs were tested for four-point bending tests with shear

spans of span/4 and span/6. Roller support was installed at one end, and pin support was installed at the other end. When a significant part of the ultimate load was applied, first slip occurred, resulting in a sudden drop in the applied load. For each specimen, the first slip load was more than the typical in-service load. As a result, all slabs failed due to a loss of the bond between the steel deck and concrete. In the post-peak zone, when there was a major deformation, a little vertical separation between the steel deck and concrete could be observed. An increase in tensile stress in the steel deck and compressive stress in concrete in the upper fibers, accompanied by a significant deflection in the slab, resulting in cracking. A sharp increase in the mid-span deflection accompanied by an end slip and wide cracks extended to the slab surface that separated the concrete compression block due to the loss of load-bearing capacity. The wide crack was located under the load application area. During the test, the adherence and slip relationship for each plate was determined, and the maximum longitudinal shear stress values calculated using the "m—k" and "partial shear" connection methods were explained and compared. Also, modeling with finite element software version 4.2.7 of ATENA 3D was included in this study to investigate the behavior of the composite slabs tested early in the laboratory. The authors developed a three-dimensional (3D) FE model to consider material nonlinearities and geometrical shapes in composite slabs. The "CC3D Interface" material type was selected, based on the Mohr-Coulomb criterion, to simulate contact between the steel deck and concrete. The interface properties in ATENA 3D consist of shear cohesion c and the coefficient of friction ϕ. It was found that the numerical models accurately and reliably predict the measured values of basic parameters of laboratory tests.

Ríos et al. (2016) developed a new finite element model, which simulates the longitudinal shear behavior of composite slabs, in Abaqus 6.12. A concrete damaged plasticity model models concrete, and the steel deck was performed as an elastic-plastic material in a static analysis chosen as the most effective analysis type. The crack inducer was included in the model, considering one of the basic requirements of Eurocode 4 and its effects on the results. 1 mm thickness crack inducer is modeled in the upper part of the concrete block, which avoids the destruction of the concrete part into two zones and the impossibility of overlapping. The controls showed that the 1 mm thickness of the crack inducer is the optimal value that does not affect the numerical solution. The Radial-Thrust connector

elements are specified to describe the relationship between steel deck and concrete, which have normal and tangential stiffness values. In such cases, a graph describing the shear stress-slip relationship during loading is used (Figure 2.7), where I— the full-shear connection, II—partial shear connection, and III- post-crushing behavior of the composite slabs.

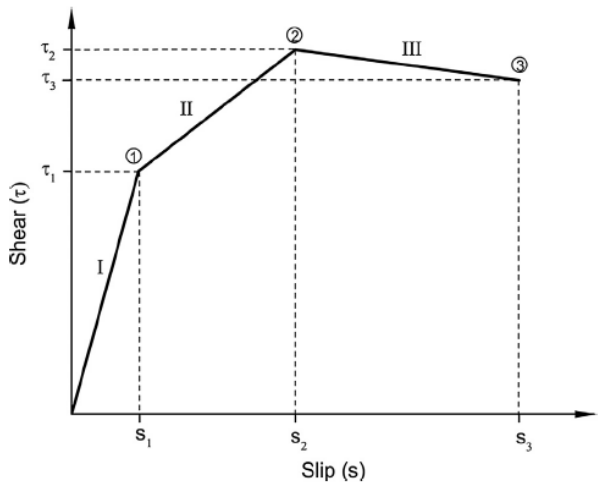


Figure 2.7. τ-s shear-bond law considered for the connector elements.

The Law of shear-bond behavior presented in Figure 2.7 affects all parameters of the composite slab, particularly on fractures in longitudinal shear, affecting primarily chemical bond, mechanical interlocking, and friction. The numerical model was evaluated by comparing it with the current experimental results of two different types of composite slabs previously tested for compliance with Eurocode 4. In addition, an interpolation method was used to get τ-s values between the steel deck and concrete for composite slabs with the similar steel deck but with different geometry and unknown shear-bond behavior.

Redzuan Abdullah et al. (2008) have made a quasi-static three-dimensional nonlinear FE model of composite slabs using ABAQUS/Explicit 6.3. To describe the relationship between the steel deck and concrete, the authors developed the Force Equilibrium method to represent the shear bond-end slip relation from bending test data. It was done to show the effect of slab slenderness on the shear bond properties of composite slabs. Solid element C3D8R is selected to model the concrete, and the shell element S4R is selected

for the steel deck. The connector element CONN3D2 is chosen to reproduce the interaction between the steel deck and the concrete, so the horizontal shear bond curve from the bending test data was assigned. The properties of materials for concrete and steel were obtained from the literature references given in Abaqus online documentation Version 6.3-1 (2002) and Hillerborg, Modeer, Peterson (1976). The Force Equilibrium method is suitable for counting the horizontal shear bond stress when two points are used in the bending test. Thus, this maximum shear bond stress is comparable with the value obtained from the Partial Shear Connection (PSC) method. An additional advantage is that the Force Equilibrium method can provide a relationship between the horizontal shear bond stress and end slip. This property can be used for numerical analysis.

Omid Monshi Toussi et al. (2016) created a numerical model of composite slabs by FEM using LUSAS software. A three-dimensional interface element was chosen to account for crack propagation and to reproduce the relationship between the steel deck and concrete. The results showed that the thickness of concrete plays a prime role in affecting the deflection at mid-span. Because as the thickness of the concrete in the slab increased, the mid-span deflection decreased accordingly. The horizontal shear resistance in slabs of different thicknesses exceeds the required shear resistance according to Eurocode Part 4, and all are within the safe range. The properties of the interface element depend on the geometry of the composite slabs.

2.6 Investigations the effect of steel fiber on the shear bond strength between elements of composite slabs

Nowadays, steel fiber is often considered an efficient substitute to steel reinforcement in the production of composite floor slabs. This is because the addition of steel fibers to the concrete increases the concrete’s energy absorption capacity, ductility, and strength in the load-bearing elements of building frames. But there is no approved design guideline of the behavior and characteristics of this type of composite slabs. Therefore, a specific SFRC mechanical model has not yet been developed and is not used in design and construction. Below are the authors who have made successful attempts to determine the effect of steel fibers on the strength and the bond between elements of composite slabs.

Foster (2009), in his study of the steel fibers effect, concluded that the tensile strength of concrete could be improved by adding steel fiber. As a result, brittle concrete will gain some plasticity, as shown in Figure 2.8. It is clear from this graph that after concrete cracks, the steel fiber promotes plastic behavior.

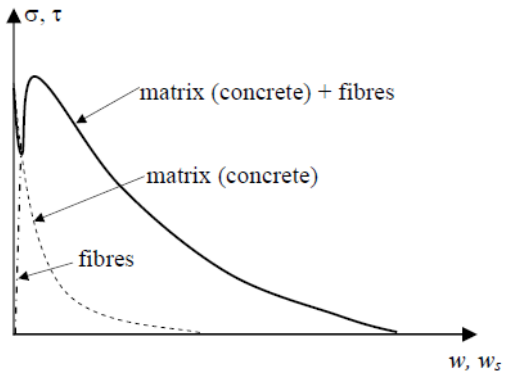


Figure 2.8. Stress versus crack opening/sliding displacement for a fiber reinforced cementitious composite (Foster 2009)

Also, on the basis of experimental studies, it was found that longer fibers and higher fiber content significantly improve the properties of concrete, particularly the energy absorption and load-carrying capacity (Khaloo and Afshari, 2005).

Petkevičius and Valivonis (2010) investigated and compared the values obtained from experimental tests of composite slabs with 20 kg/m^3 of steel-fiber and plain concrete. The built-up bars method, which was previously created by Vainiunas et al. (2006), was used to evaluate the results. Modifications have been made by this method, such as changing the interface rigidity from plain concrete to steel-fiber concrete. As a result of the comparison, the authors concluded that the slip loads of steel-fiber concrete were 50% to 60% higher than composite slabs with plain concrete. But at the same time, the influence of dosage and size of steel fiber was neglected.

Fairul Zahri Mohamad Abas (2014, Sydney) investigated experimentally and numerically the strength of composite slabs with varying amounts of steel fiber. One-span and two-span composite slabs were selected with deep trapezoidal profiled steel decking. The steel

fibers were 60 mm long end-hooked fibers. For fracture and shear bond strength tests between concrete and profiled steel, composite slabs were tested using plain concrete and steel fiber reinforced concrete (SFRC), with fiber dosages of 20 kg/m^3, 30 kg/m^3, 40 kg/m^3, and 60 kg/m3. Using the Daniels and Crisinel Fairul Zahri Mohamad study results, Abas successfully modeled the bond-slip relationship between the steel deck and concrete (for plain concrete and steel fiber reinforced concrete). For the material property of the concrete CDP model was used. In the simulation of this model, the shear bond at the first slip had a significant influence. It was used to predict the initiation of the first slip between the decking and the concrete in all other composite slabs. The maximum bond shear stress values predicted by the numerical model were in reasonable agreement with the shear stress estimated from the experimental results.

3. MATERIALS and METHODS

This chapter illustrates a simulation of the longitudinal shear behavior of composite slabs. Developing an authentic 3D finite element (FE) model that can reproduce the behavior of composite slabs under monotonic loading and be comparable to experimental results was the main goal. The model was developed using ABAQUS/CAE (ABAQUS Manual 2012). The geometry, assembly, material properties, mesh, loading, boundary conditions, steps, and interactions are discussed. Also, the modeling procedure and method used by ABAQUS are discussed in detail.

3.1 General Description of Finite Element Method

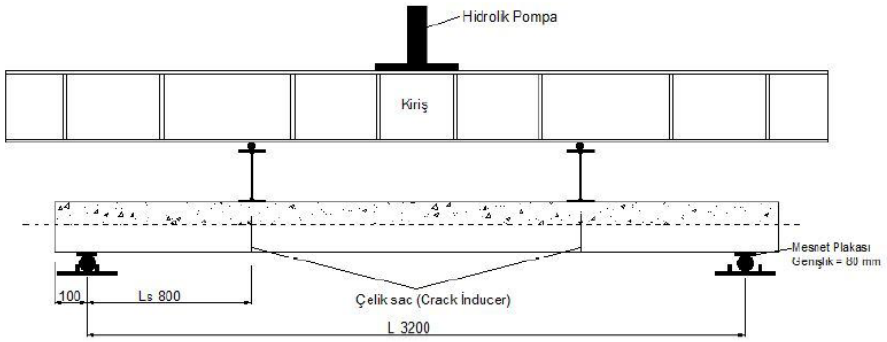
Originally, the finite element method was designed to solve problems concerning solid-state mechanics, but later it got widespread use in computational physics and engineering areas. Fields as conventional structural analysis, heat transfer, mass transfer, fluid flow, and potential electromagnetic are the typical areas of interest. Nowadays, FEM is considered the most flexible method. Therefore, it can be used as a universal tool for a wide range of numerical problems. The main idea of the FEM can be represented as dividing the computational area into smaller parts to find local solutions that satisfy the differential equation within this area. By combining individual solutions on these parts, a global solution can be obtained (Bastian E. Rapp 2017).

The disadvantage of FEM is the existence of specific requirements, which makes it necessary to search for a compromise between accuracy and computation speed. The study or analysis of a phenomenon using FEM is often referred to as finite element analysis (FEA).

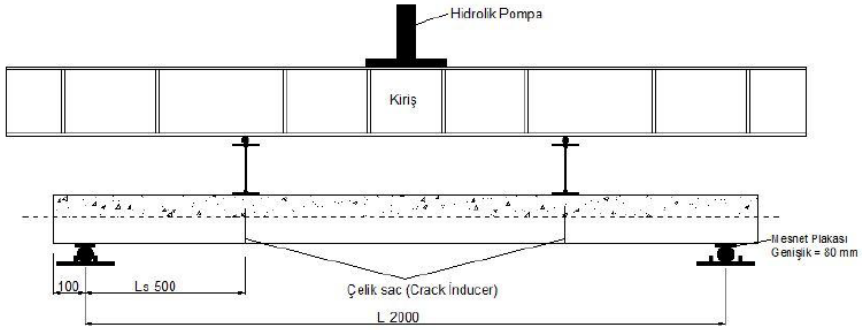
3.2 Finite Element Model

In this section, descriptions of the modeling procedure of composite slabs by ABAQUS are given.

The supporting and loading system used for experiment tests is represented in Figure 3.1. Also, considering one of the requirements of Eurocode 4, crack inducers were included in the model.



(a) long slab



(b) short slab

Figure 3.1. The supporting and loading system of experiment tests: a) long slab; b) short slab (Başsürücü 2013).

3.2.1 Modeling and Model Geometry

ABAQUS software has different modules that would provide us with the required tools to model our structure. "Part" module of Abaqus is essentially the initial module where starting the modeling process of any structure.

The geometry of composite slabs and fiber content used in the experiment are given in Table 3.1. Figure 3.2 shows the steel deck's section.

Table 3.1. Properties of composite slabs (Başsürücü 2013).

Composite flooring sample properties							
Slab	L (mm)	L_0 (mm)	L_s (mm)	h_f (mm)	b (mm)	Ap (mm^2)	The amount of steel fibers (kg/m^3)
CS-1	3200	100	800	150	900	1200	-
CS-2	3200	100	800	150	900	1200	-
CS-3	3200	100	800	150	900	1200	-
CS-4	2000	100	500	150	900	1200	-
CS-5	2000	100	500	150	900	1200	-
CS-6	2000	100	500	150	900	1200	-
CS-7	3200	100	800	150	900	1200	40
CS-8	3200	100	800	150	900	1200	80
CS-9	3200	100	800	150	900	1200	120

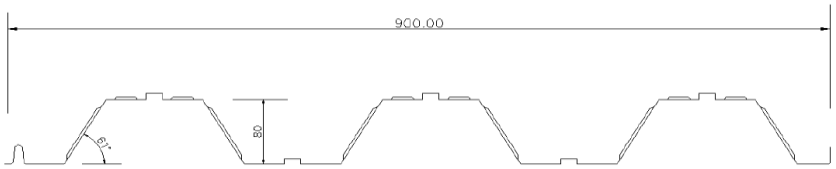


Figure 3.2. The steel deck parameters (Başsürücü 2013)

Six independent parts (Figure 3.3.) corresponding to the steel deck, two crack inductors, and three concrete blocks were modeled in the Part section, and then they were assembled in the "Assembly" section (Figure 3.4.).

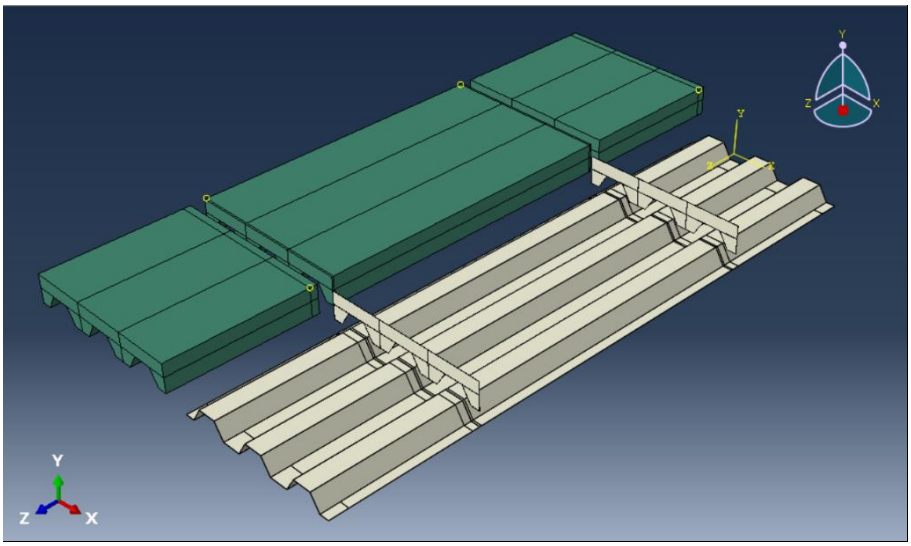


Figure 3.3. Six independent parts

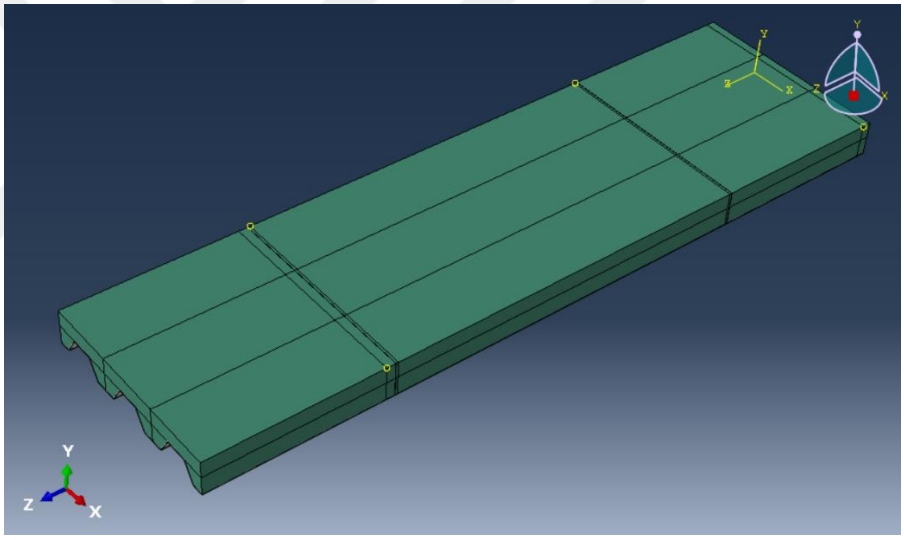


Figure 3.4. Model assemblage

The concrete blocks consist of solid deformable elements C3D8R by extrusion type, and the steel deck is discretized with shell deformable elements S4R by extrusion type too. C3D8R are three-dimensional hexahedral elements of 8 nodes. S4R is a general-purpose quadrilateral element of 4 nodes (Figure 3.5).

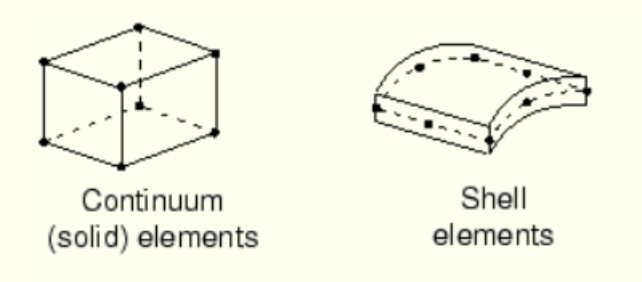


Figure 3.5. Type of elements (ABAQUS Manual 2012)

Due to the symmetry of the system, a quarter of the structure is modeled, as shown in Figure 3.6.

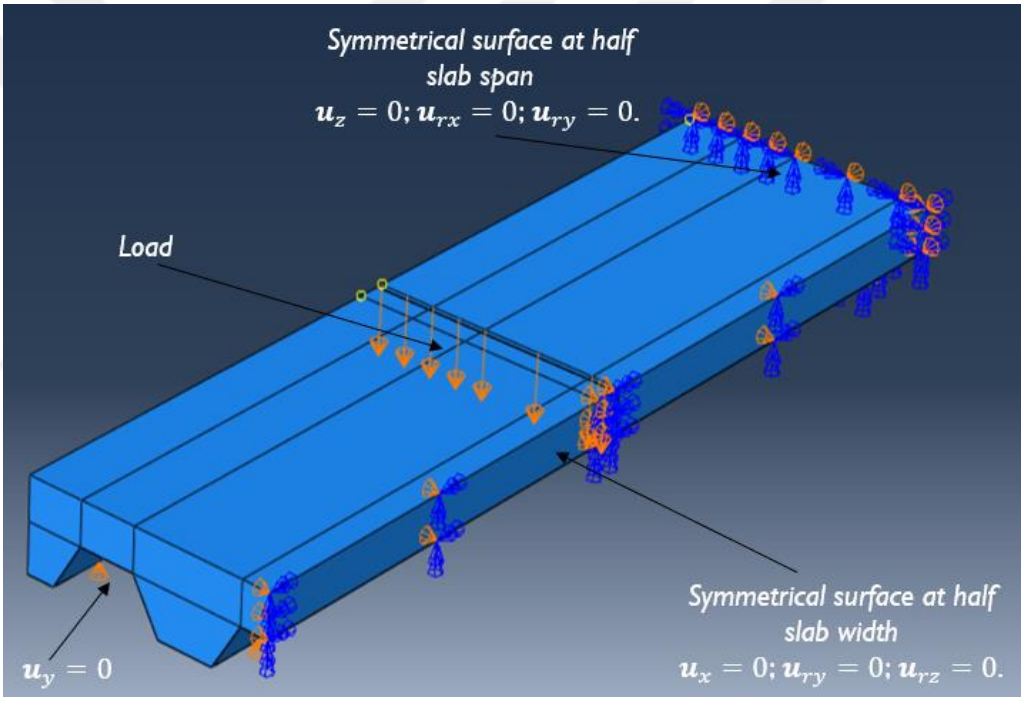


Figure 3.6. A quarter of the composite slab

3.2.2 Material Properties

This section describes the properties of the materials used to model the composite slab. The main goal of material modeling was to develop solid material models that accurately predict the behavior of composite slabs with plain concrete and concrete with steel fibers under applied load. It was essential to obtain a reliable numerical model that accurately mimicked the behavior observed in the laboratory. Experimental material properties and established material models from the literature were used to develop an accurate material behavior model. Material properties for concrete and steel are defined in the Abaqus "Define material" module and assigned to the relevant elements.

Concrete

It is hard to capture the fundamental behavior of concrete using elastic damage models or the laws of elastic plasticity because irreversible deformations cannot be taken into account in the elastic damage model. As seen in Figure 3.7 (b), zero stress corresponds to zero strain, resulting in an overestimation of the damage amount. However, when an elastic-plastic relationship is assumed, the deformation will be overestimated as the unloading curve will follow an elastic slope (Figure 3.7 (c)). Thus, a Concrete Damage Plasticity (CDP) model combining these two approaches may reflect the behavior of experimental unloading (Figure 3.7 (a)) (Jason et al., 2004).

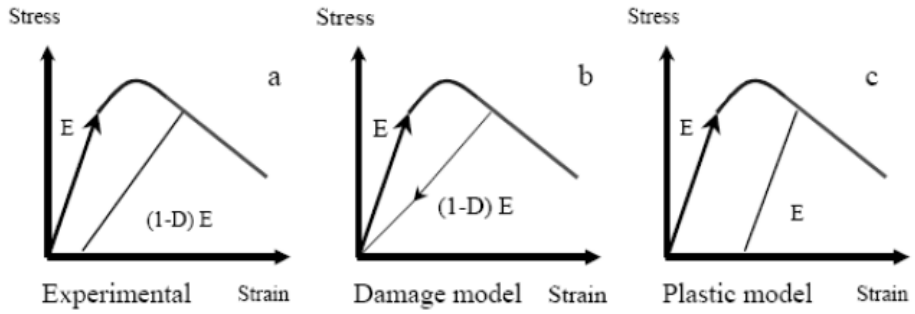


Figure 3.7. Elastic plastic damage law (Jason et al. 2004)

In this thesis, Concrete Damage Plasticity (CDP) model was chosen to simulate the plain concrete and concrete with steel fibers.

CDP model consists of two main failure mechanisms: compressive crushing and tensile cracking. The change of the yield surface is controlled by equivalent plastic deformations in tension and compression (Figure 3.8).

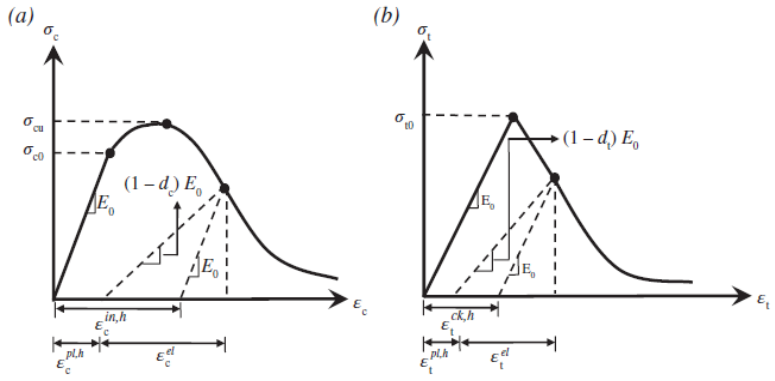


Figure 3.8. Response of concrete to a uniaxial loading condition: (a) Compression, (b) Tension (ABAQUS Manual 2012).

The values obtained from the experiments often are represented by nominal stress and nominal strain. But in the case of CDP, when determining plasticity data in Abaqus, true stress and true strain must be used to interpret the data correctly.

The first step is to use equations that convert nominal stress and nominal strain to true stress and true strain. The relationship between true strain and nominal strain is shown as:

$$\varepsilon_{true}=\text{In}\,(1+\varepsilon_{nom}) \tag{3.1}$$

The relationship between true stress and nominal stress is calculated as:

$$\sigma_{true}=\sigma_{nom}\,(1+\varepsilon_{nom}) \tag{3.2}$$

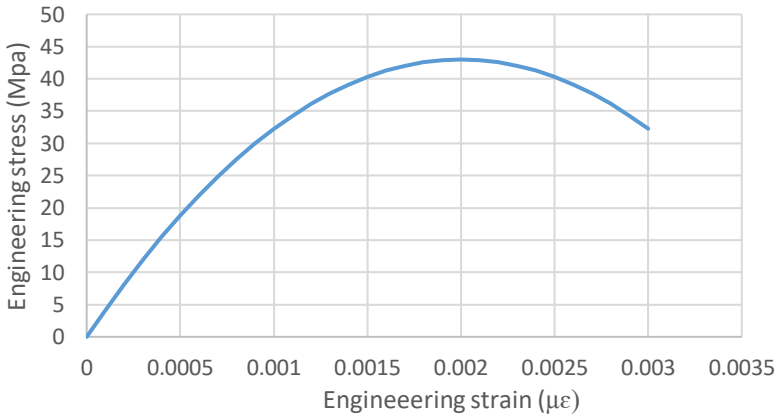
The next step is to use equations relating plastic strain to total and elastic strains to specify the plastic strains associated with each yield stress value. The plastic strain values that are given to Abaqus while defining plasticity is calculated from the relationship written as:

$$\varepsilon^{pl} = \varepsilon^{t} - \varepsilon^{el} = \varepsilon^{t} - \sigma_{true}/E \tag{3.3}$$

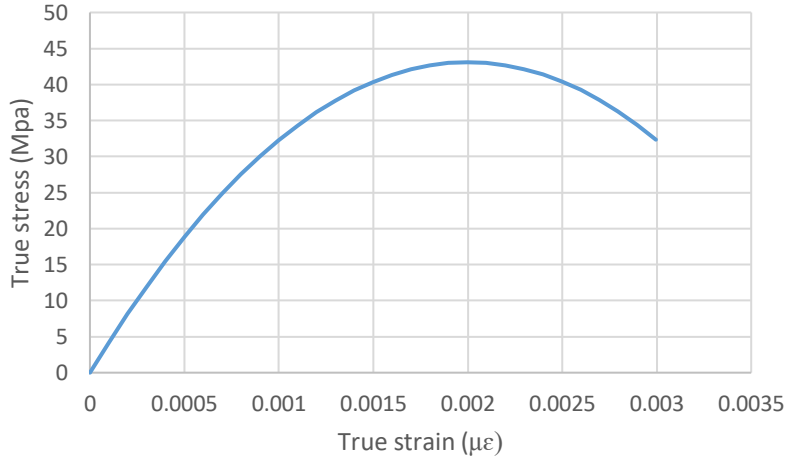
where d_t and d_c are two scalar damage variables, ranging from 0 (no damage) to 1 (fully damaged). The damage model used for concrete was based on ductility and took into account tensile and compression fracture. In consideration of d_c increases compared to an increase in $\varepsilon^{in,h}{}_c$, could be expressed as follows:

$$d_c = 1 - \sigma_c / \sigma_{max.\ true} \tag{3.4}$$

According to compressive stress of concrete from laboratory tests and formulas above, all needed data was converted. Figure 3.9 and Figure 3.10 show engineering and true data for concrete B43 (plain concrete).

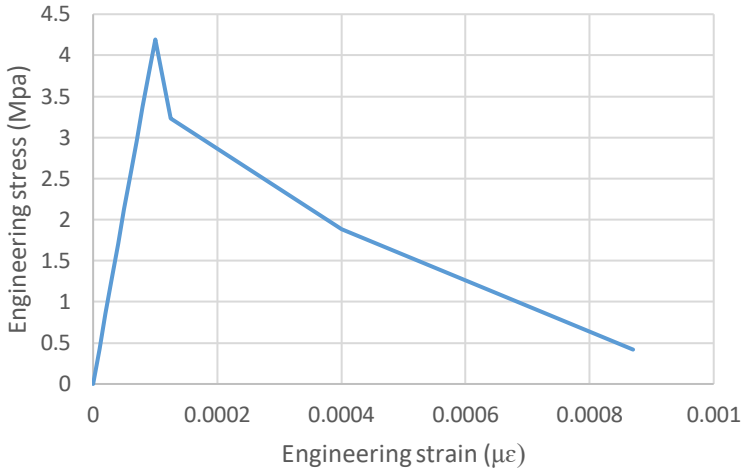


(a)

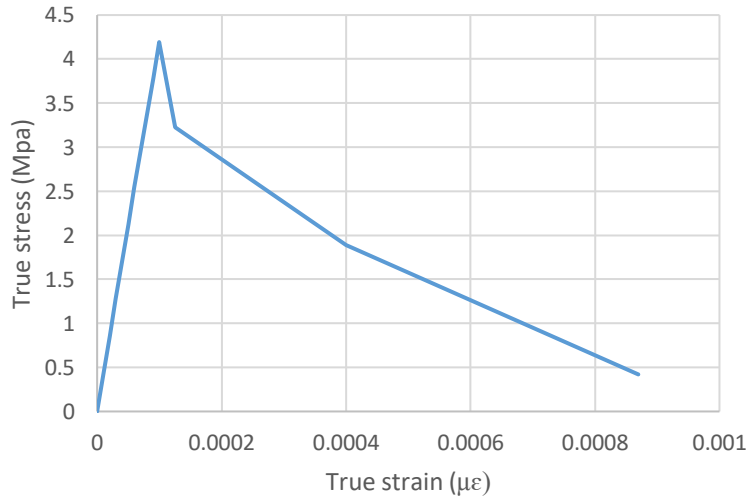


(b)

Figure 3.9. Compression curves of concrete B43: (a) Engineering stress versus engineering strain, (b) True stress versus true strain.



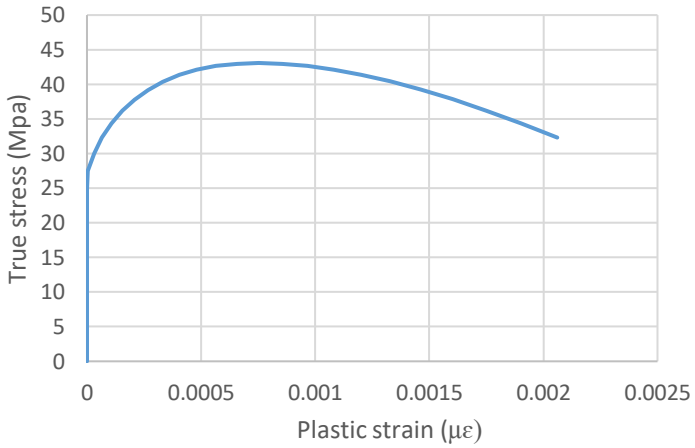
(a)



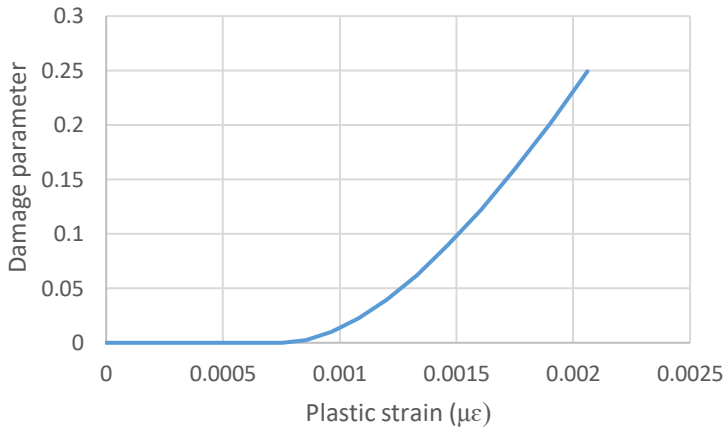
(b)

Figure 3.10. Tension curves of concrete B43: (a) Engineering stress versus engineering strain, (b) True stress versus true strain.

Then by Equation 3.3, the true strain was converted to plastic strain, which was used in Abaqus (Figure 3.11 (a) and Figure 3.12 (a)). Also, damage parameters were obtained by Equation 3.4 (Figure 3.11 (b) and Figure 3.12 (b)).

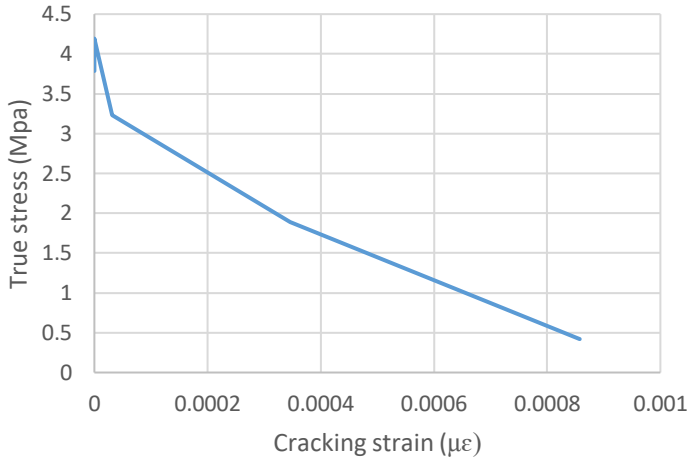


(a)

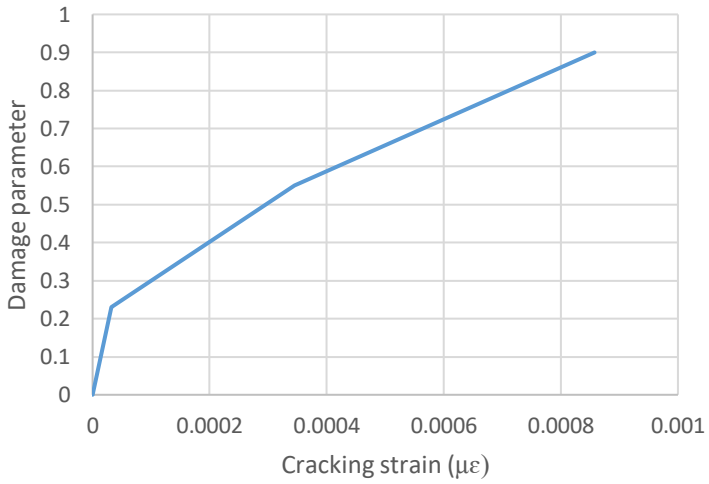


(b)

Figure 3.11. Compression curves of concrete B43: (a) True stress versus plastic strain, (b) Damage parameter versus plastic strain.



(a)



(b)

Figure 3.12. Tension curves of concrete B43: (a) True stress versus cracking strain, (b) Damage parameter versus cracking strain.

Other classes of concrete were calculated in the same way using given equations.

Steel

There are several models in Abaqus for analyzing metal ductility. The main options are rate-independent and rate-dependent plasticity, the von Mises yield surface for isotropic materials, the Hill yield surface for anisotropic materials, and the isotropic and kinematic hardening for rate-independent modeling (ABAQUS Manual 2012).

Isotropic hardening was chosen. Isotropic hardening provides equally changing of the yield surface size in all directions. Consequently, yield stress increases (or decreases) in all stress directions, and plastic deformation occurs. Using an isotropic hardening model is helpful for large plastic deformation situations and in situations when deformation occurs at all points in essentially the same direction in the deformation space throughout the analysis. Although the model is called the "hardening" model, it is possible to define it as deformation softening or softening following hardening (ABAQUS Manual 2012).

If isotropic hardening is specified, yield stress can be determined as a tabular function of plastic deformation and, if necessary, temperature and/or other predefined field variables. The yield stress at a given state is simply interpolated from this data sheet and remains constant for plastic strains greater than the value in the last table.

To input steel parameters, it is necessary for the nominal stress and strain to convert by Equation (3.1) and Equation (3.2). The converted data are shown in Tables 1 and 2. Data used in Abaqus is presented in Figure 3.13.

Table 3.2. Parameters of steel: (a) engineering data; (b) true data.

Engineering data	
σ - stress (Pa)	ε -strain
0	0
340000000	0.001619
340000000	0.004

(a)

True data	
σ - stress (Pa)	ε -strain
0	0
340550460	0.001618
341360000	0.003992

(b)

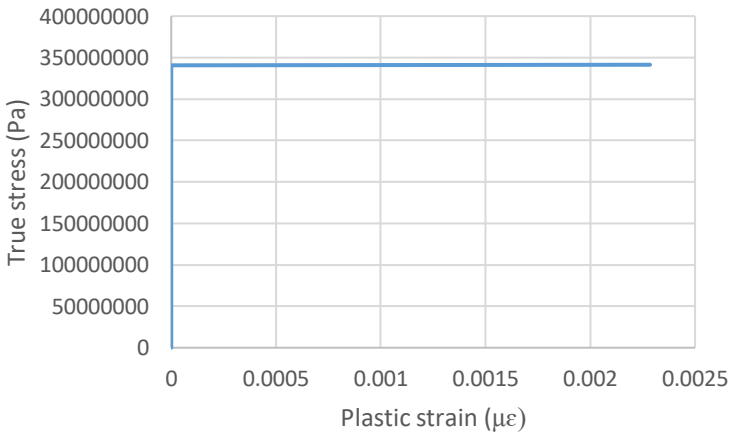


Figure 3.13. Steel parameters used in Abaqus.

Material properties are modeled with elastic-plastic behavior considering nonlinearity to obtain plastic effects.

3.2.3 Step

There are two primary analysis methods used for solving structural problems in Abaqus, namely Explicit (ABAQUS / Explicit) and Implicit (ABAQUS / Standard). A traditional stiffness-based solution method consisting of the full Newton-Raphson iterative approach for solutions of equilibrium equations is used in the implicit algorithm. It is a suitable method to solve various static problems, especially for problems that do not experience severe nonlinearity in geometric or material behavior.

ABAQUS / Explicit has the opposite characteristics. ABAQUS / Explicit can simulate highly non-linear behavior involving cracking of the concrete, excessive displacement and distortion, and loss of contact interface (ABAQUS Manual 2012; Chaudhari and Chakrabarti 2012; Watts, Kayvani et. al. 2013). However, ABAQUS/Explicit was developed to simulate dynamic analysis. But later, many researchers found ABAQUS / Explicit useful in solving static and quasi-static engineering problems. (Sun, Lee et. al., 2000; ABAQUS Manual 2012). Common engineering problems are associated with a high degree of non-linearity in geometry and materials. It also concerns composite slabs' design because of non-linear material properties. As a result, concrete cracks, which lead to a significant decrease in stiffness with increasing load. Besides, the complex interaction between profiled steel deck and concrete produces highly non-linear behavior, which is challenging to model using the implicit method (Abas 2014).

Considering the reason given above, ABAQUS/Explicit was chosen to analyze the composite slab model. ABAQUS/Explicit was selected to simulate the non-linearity of material and geometric and the non-linear behavior of the contact surface between the profiled steel deck and the concrete. The algorithm has a simple yet comprehensive method for validating data throughout the analysis, entering pre-processing, and outputting post-processing results. Previously, many other researchers have also used this software due to its simplicity and capabilities, especially for composite structures (Shanmugam, Kumar et.al. 2002; Qureshi, Lam et. al. 2011; Ellobody and Young 2006; Abbas and Mohsin 2012; Abdullah and Easterling 2012; Lian, Uy et.al. 2005).

3.2.4 Incremental loading

There are two ways of changing the load value throughout the step (linearly changing load and constant load). Depending on the analysis, different amplitude curves are selected to determine changes over time.

In this model, the composite slabs are loaded by applying controlled vertical displacement in the form of two linear loads moving at a distance of L/4 from the supports. The tabular definition method is chosen to specify an amplitude curve in a table of values at appropriate points along the timeline. Abaqus performs a linear interpolation between these values as needed. However, Abaqus/Explicit does not use default smoothing. But using the smooth step definition method promotes more accuracy and efficiency results of loading because sudden movements cause inaccurate solutions. Therefore, in this work, a smooth amplitude function used the tabular definition method was applied (Figure 3.14). Acceleration of displacement needs to change slightly from zero to the maximum value for the load to be applied most evenly. If the acceleration is smooth, the velocity and displacement changes are also smooth (ABAQUS Manual 2012).

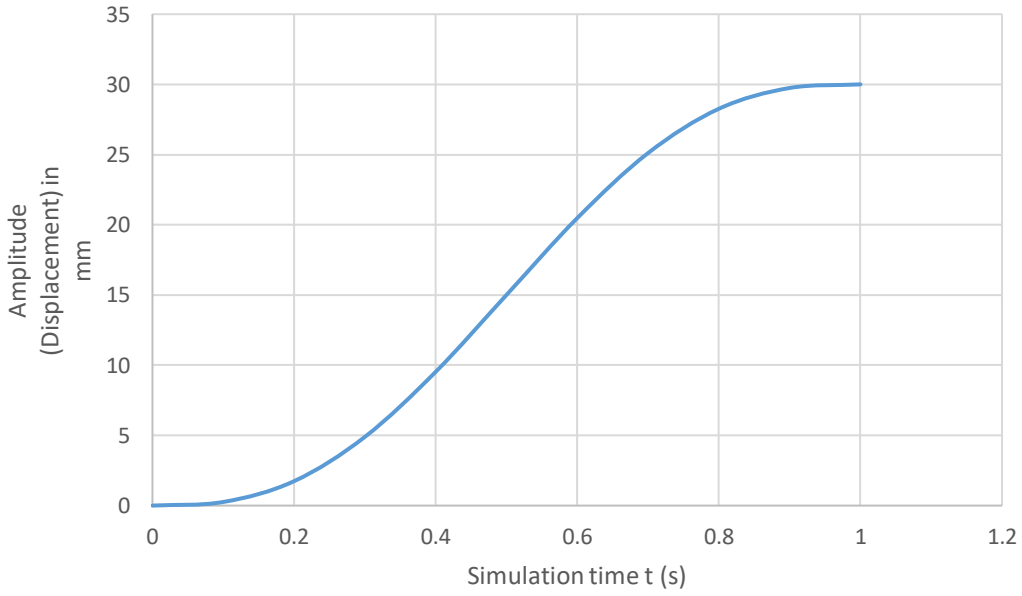


Figure 3.14. Smooth amplitude (displacement) curve to control the applied displacement (ABAQUS Manual 2012).

The calculation of amplitudes based on the smooth step data is used for creating a smooth amplitude curve. For counting the amplitude, *a*, between two consecutive data points (t_i, A_i) and (t_{i+1}, A_{i+1}) next equation is represented:

$$a= A_i+(A_{i+1}- A_i)\xi^3(10-15\xi+6\xi^2) \text{ for } t_i \leq t \leq t_{i+1}, \quad (3.4)$$

where $\xi= (t- t_i)/(t_{i+1}- t_i)$.

A and t are the amplitude (or displacement) and time of simulation, respectively. Thus, from the above function, $a= A_i$ at t_i, $a= A_{i+1}$ at t_{i+1}, and the first and second derivatives of a are equal to zero at t_i and t_{i+1}. This definition is for a smooth increase and decrease from one amplitude value to the next.

The amplitude, a, is defined such that:

$$a= A_0 \quad \text{for} \quad t \leq t_0, \quad (3.5)$$

$$a= A_f \quad \text{for} \quad t \geq t_f, \quad (3.6)$$

where (t_0, A_0) and (t_f, A_f) are the first and last data points, respectively.

The ABAQUS/Explicit used a smooth amplitude function to maintain a very low inertia effect to reach a quasi-static state. The maximum displacement of 30 mm was applied to the composite slab to simulate the mid-span deflection beyond the peak load. The total time required to simulate a quasi-static solution was 1 second.

3.2.5. Detailed description of all interactions

One of the main goals was to capture the most realistic relationship between concrete and steel deck surfaces (shown in Figure 3.15). This interaction should be close to real conditions as possible. Below in this chapter, interactions between crack inducers, concrete, and steel deck were discussed.

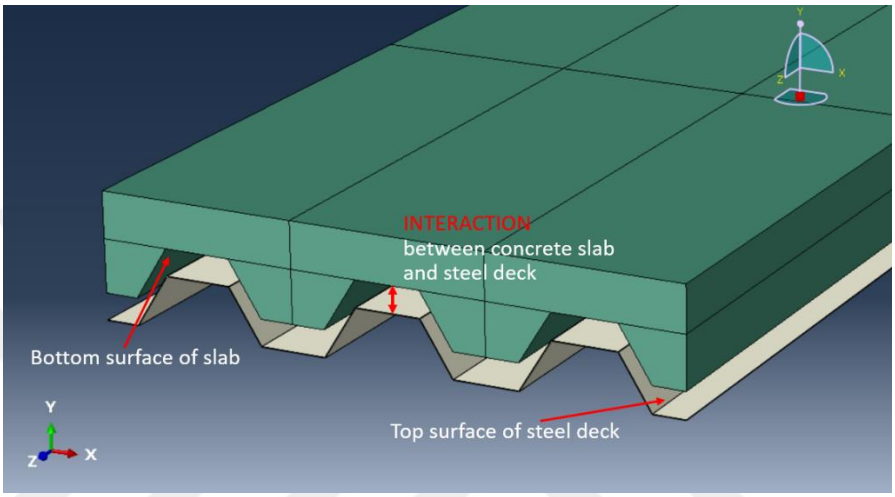


Figure 3.15. Interaction between concrete slab and steel deck

Interaction between steel deck and concrete

According to an earlier study by Chen and Shi (2011), there is an adhesion (chemical) bond between the steel deck and concrete before sliding. This bond prevents slip between the steel deck and concrete until the shear stress reaches a certain threshold of τ_{slip} where the first slip occurs. After the appearance of the first slip, the effect of the chemical bond deteriorates. Figure 3.16, compiled by Daniels and Crisinel (1993), illustrates this behavior in detail. Daniels and Crisinel conducted the pull-out tests of composite slabs and represented typical interface behavior consisting of initial chemical bonding and frictional behavior.

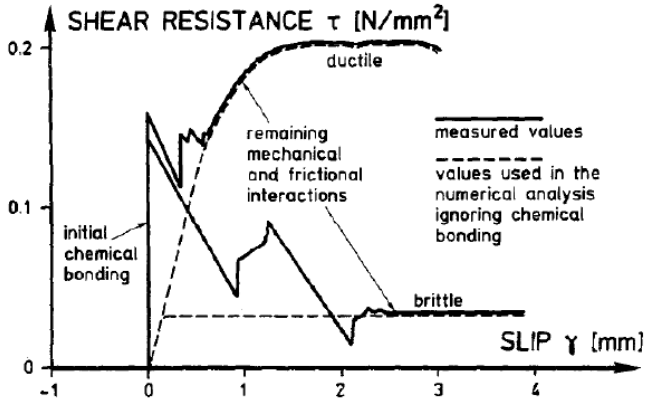


Figure 3.16. Typical shear resistance versus slip behavior of composite slab (Daniels and Crisinel 1993).

The next stage is characterized by the appearance of a mechanical interlock work, which leads to friction between the surfaces. Mechanical interlock is the shape of embossment or any indentation present on the surface of a profiled steel deck. So mechanical interlock increases the longitudinal shear strength until the concrete slab completely overcomes the relief (Schuster and Ling 1980; Wright 1998; Veljkovic 1996; Chen and Shi 2011).

Previously, in the process of modeling composite slabs by FEA, many researchers ignored the effect of the adhesive bond and paid more attention to ultimate longitudinal shear strength τ_u. But Fairul Zahri Mohamad Abas (2014) showed the adhesive bond is important. The author hypothesized that the first slip causes a significant loss of stiffness and the composite slab is no longer usable after reaching the slip load.

Based on experimental and numerical studies, two stages of behavior between concrete and deck have been identified and modeled:

1. The first stage is the stage before the start of the first slip. At this stage, any considerable slipping does not occur because the chemical bond prevents it. Furthermore, no residual damage remains on the composite slab after unloading. This behavior is linear.

2. The second stage is a stage after the first slip occurred. At this stage, significant sliding is observed at one or both ends of the composite slab. This behavior is non-linear because residual damage remains after unloading.

Definition of interaction according to 2 stages

General Contact interaction was chosen to model the two stages described above (Figure 3.17).

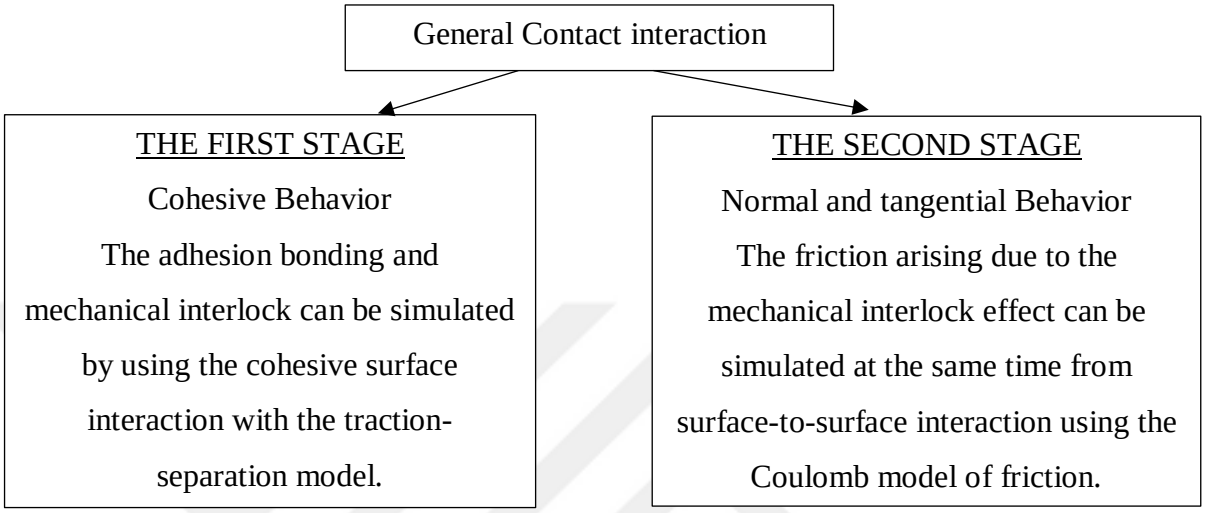


Figure 3.17. General Contact interaction

The first stage is represented by cohesive behavior and damage to simulate adhesion bond and mechanical interlock. In ABAQUS/Explicit, it was done by using the traction-separation model.

The second stage consists of Tangential and Normal behaviors. In this case, to model simultaneously rising friction and the mechanical interlock effect, surface-to-surface interaction using the Coulomb model of friction was selected.

Every interaction behavior described above between elements is discussed below.

Cohesive behavior

The method described here can be used to model connected interfaces that may have the possibility of damage or failure. Other features, including cohesive elements, have similar functions and could be used for connected interfaces. The same data must be set in the material properties for using cohesive elements or other element types. But using cohesive contact behavior is essentially more effortless and allows to simulate of a wide range of contact connections (for example, two sticking elements in contact during analysis). One of the main reasons for using cohesive contact behavior is the small value of the interface thickness. The definition of a damage model for cohesive behavior provides a simulation of an associated interface that may fail due to loading (ABAQUS Manual 2012).

Since the adhesive bond is linear at the first stage, the traction-separation model in Abaqus was chosen. The traction-separation model consists of an initially linear elastic part, the initiation, and the evolution of damage (Figure 3.18).

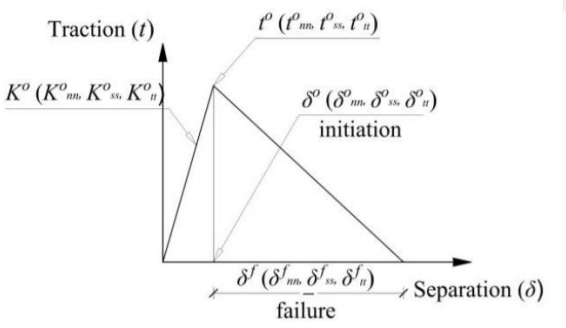


Figure 3.18. Typical traction-separation response.

The indices *n, s,* and *t* define the normal and the two shear directions. K_{nn}, K_{ss} and K_{tt} are the cohesive surface stiffness in the normal and two shear directions. t_n^0, t_s^0, t_t^0 and δ_n^0, δ_s^0, δ_t^0 are the tractions and separations, respectively. When these values reach the peak, damage starts. This damage becomes maximum when analysis goes until δ_n^f, δ_s^f, δ_t^f which means failure.

Based on these values of tractions and separations, the elastic behavior can be described as the matrix (ABAQUS Manual 2019):

$$\underline{t = \begin{Bmatrix} t_n \\ t_s \\ t_t \end{Bmatrix} = \begin{bmatrix} K_{nn} & K_{ns} & K_{nt} \\ K_{ns} & K_{ss} & K_{st} \\ K_{nt} & K_{st} & K_{tt} \end{bmatrix} \begin{Bmatrix} \delta_n \\ \delta_s \\ \delta_t \end{Bmatrix} = K_\delta} \tag{3.7}$$

For a more detailed understanding of the directions, three different failure modes are considered. Therefore, each direction corresponds to a particular mode: n –direction is Mode 1, a normal-opening mode; s –direction is Mode 2; t-direction is Mode 3 (Figure 3.19).

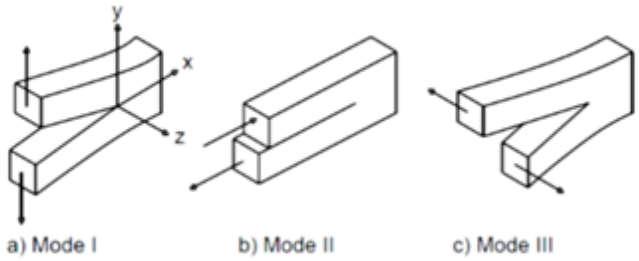


Figure 3.19. Different types of failure modes (Björnström et al. 2006)

According to Diehl's research (2004), the value of K_{nn} coefficient should be around 1000 N/mm. Small or too high a value of stiffness can be a reason for numerical instability. Since damage due to Mode 3 is not expected, K_{tt} coefficient can be taken big enough, as K_{nn}. K_{ss} is calculated using t_s^0 and δ_s^0, because in this direction, slipping occurs. This direction is responsible for longitudinal shear strength. For composite slabs with deep trapezoidal profiled steel deck and plain concrete, the typical value of shear stress at first slip t_s^0 is between 0.074 N/mm ^{2} to 0.094 N/mm^2 (Burnet and Oehlers 2001).

The value of δ_s^0 is displacement, after which slipping occurs, and it is taken as 0.1 mm. (as per Eurocode 4 (EN1994-1-1:2005)). In this thesis, for plain concrete t_s^0 is taken as 0.08 N/mm ^{2}; therefore, K_{ss} is 0.8 (Figure 3.20).

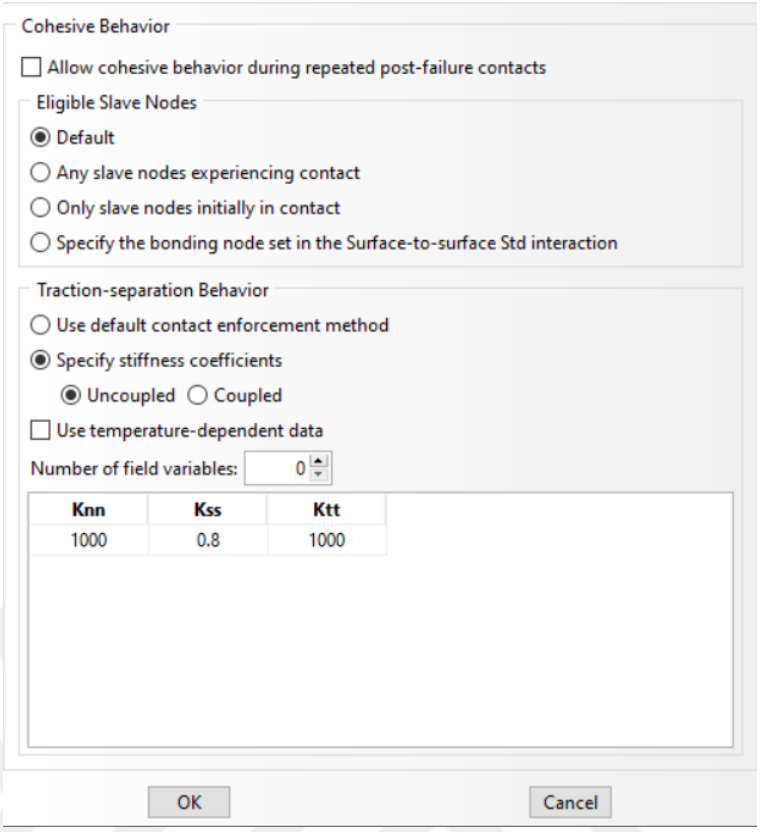


Figure 3.20. Cohesive Behavior defined between the steel deck and plain concrete.

Friction behavior between the steel deck and concrete

As previously described, after the first slip occurs (adhesion bond ended), the friction behavior and mechanical interlock begin to resist the loss of load-bearing capacity of the composite slab. Friction between surfaces appears when the mechanical interlock starts to engage. Frictional behavior is simulated by using The Coulomb model of friction (Figure 3.21). This model relating the friction shear stress τ_f to the normal contact N between the steel deck and concrete is determined by the formula:

$$\tau_f=\mu N \tag{3.8}$$

where μ is the coefficient of friction. The value of μ is between 0.4 to 0.6 (Eurocode 4).

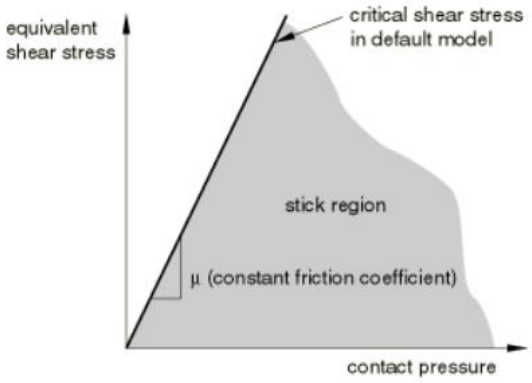


Figure 3.21. Slip regions for the basic Coulomb friction model (ABAQUS Manual 2012)

In this study, the friction coefficient is taken 0.4 (Figure 3.22).

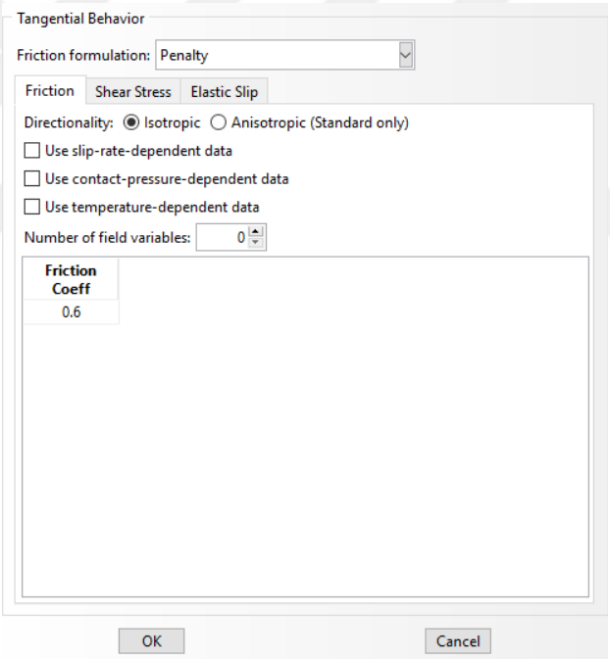


Figure 3.22. Frictional Behavior

In addition, in this stage, Normal behavior has been assigned as “Hard” contact (Figure 3.23). It means that in case the contact pressure between surfaces is zero, the surfaces separate.

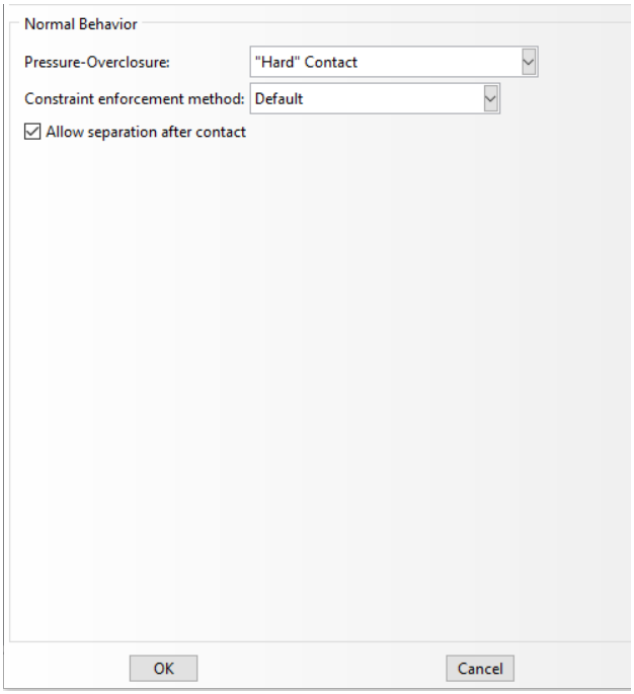


Figure 3.23. Normal Behavior

Failure criteria of contact

The damage model provides to model the degradation and eventual destruction of the bond between the two connected surfaces. Damage requires the assignment of two criteria: a damage initiation criterion and a damage evolution law. If the damage initiation criterion is not introduced to describe the damage evolution, Abaqus may assume no damage in the material. Damage can occur when the damage initiation criterion is defined according to a user-defined damage evolution law. In this work Maximum stress criterion is used for assigning the damage initiation. Damage initiation begins when the maximum contact stress ratio is one:

$$max\left\{\frac{\langle t_n \rangle}{t_n^0}, \frac{t_s}{t_s^0}, \frac{t_t}{t_t^0}\right\} = 1 \tag{3.9}$$

As several modes of failure are not possible simultaneously for cohesive surfaces, only one damage initiation criterion and damage evolution law is available. In this study, failure occurs because of longitudinal shear strength as a result of sliding. Therefore, mode 2 of failure is considered. From the above, it can be concluded that the damage initiation will occur when shear stress t_s^0 is between 0.074 N/mm ^{2} to 0.094 N/mm ^{2}. It

means at the same time, when the first slip occurs, damage initiates. t_n^0 and t_t^0 should be taken high for pretending failures in this direction. Consequently, in directions *n* and *t* slip will not occur, and behavior will be every time in elastic mode. Damage initiation of the composite slab with plain concrete is presented in Figure 3.24.

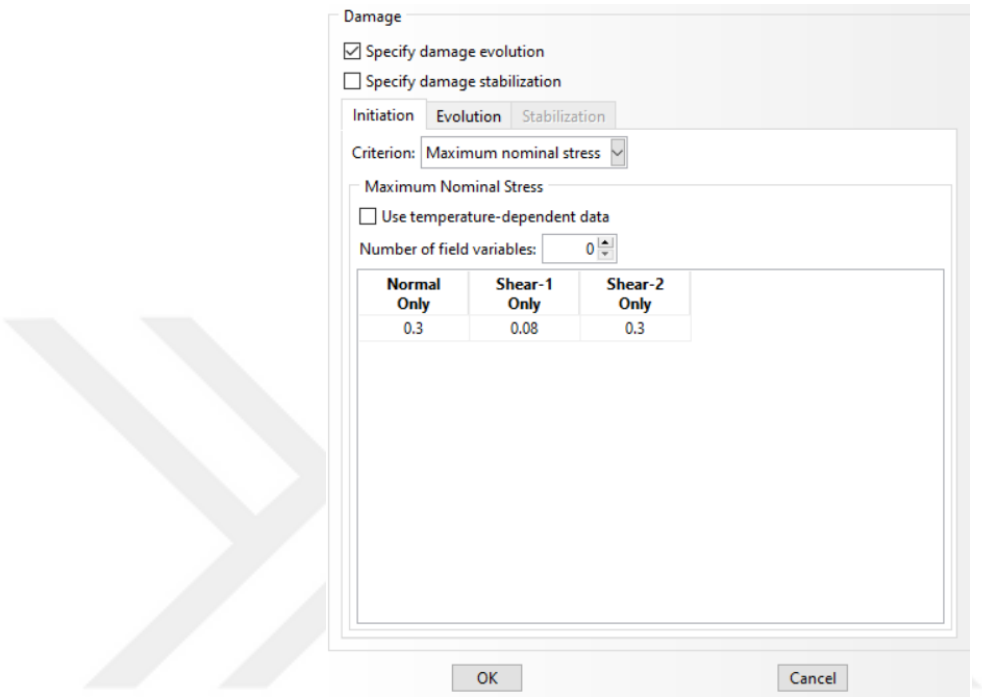


Figure 3.24. Damage initiation of composite slab with plain concrete.

After the damage is initiated, the shear stresses of the adhesive bond decrease at a deterioration rate specified at damage development law (ABAQUS Manual 2012). The degree of this degradation is determined by a scalar damage variable D, which at a zero value means no damage, and a value of 1 represents the destruction of the contact. Decreased contact stress or traction values can be calculated using the formula:

$$t_{n,s,t} = (1 - D)\bar{t}_{n,s,t},$$
$$\bar{t}_{n,s,t} \geq 0 (otherwise\ no\ damage \text{ to compressive stiffness}) \qquad (3.10)$$

where $t_{n,s,t}$ are the contact stress components predicted by the elastic traction-separation behavior for the current separations without damage (ABAQUS Manual 2012).

Abaqus offers to use an effective separation δ_m for specifying the evolution of damage under a combination of normal and shear separations across the interface:

$$\delta_m = \sqrt{\langle \delta_n \rangle^2 + \delta_s^2 + \delta_t^2} \tag{3.11}$$

For simulating damage evolution, a linear function was preferred. The selected linear softening curve is represented by Equation 3.12 and depends on mechanical interlock parameter δ_m^f.

$$D = \frac{\delta_m^f(\delta_m^{max} - \delta_m^0)}{\delta_m^{max}(\delta_m^f - \delta_m^0)} \tag{3.12}$$

It can be seen from the formula that complete contact failure happens, and the shear stress limit reaches the maximum when the mechanical interlock is full overcome. The mechanical interlock parameter δ_m^f depends on the width of the embossments. The typical value of the mechanical interlock can range from 5 mm to 20 mm, depending on the size of the embossment or indentation on the surface of the steel deck.

Slip shear strength τ_{slip} for composite slabs with steel fiber

As discussed earlier, the first of sliding occurs when the longitudinal shear strength reaches a critical value τ_{slip} and the adhesive bond between the concrete and the surface of the profiled steel sheet is destroyed. In the case of flat concrete composite slabs, the τ_{slip} value is determined from the push-out test results. Many studies have shown that steel fibers improve the post-cracking behavior of a concrete member (Foster 2012) and slow the development of shear in composite sheets.

This study assumes that the shear strength τ_{slip} for the steel fiber composite sheet is directly proportional to the tensile stress σ_t at the beginning of shear. Therefore, the increase in shear strength with increasing steel fiber dosage in concrete can be expressed as:

$$\tau_{slip} = \tau_{0,plain} + \tau_{0,sfrc} \tag{3.13}$$

where $\tau_{0,plain}$ is the shear bond stress at slip for a composite slab with plain concrete, $\tau_{0,sfrc}$ is the increase of shear bond stress from the contribution of steel fibers.

Voo and Foster (2012) developed the Variable Engagement Model (VEM) for the steel-fiber reinforced concrete (SFRC), which describes the unloading behavior of SFRC under tensile stress. This law of steel-fiber reinforced concrete in tension consists of two components, as shown in Figure 3.25. The first component is the strength of the concrete matrix, and the second is the contribution of the steel fibers.

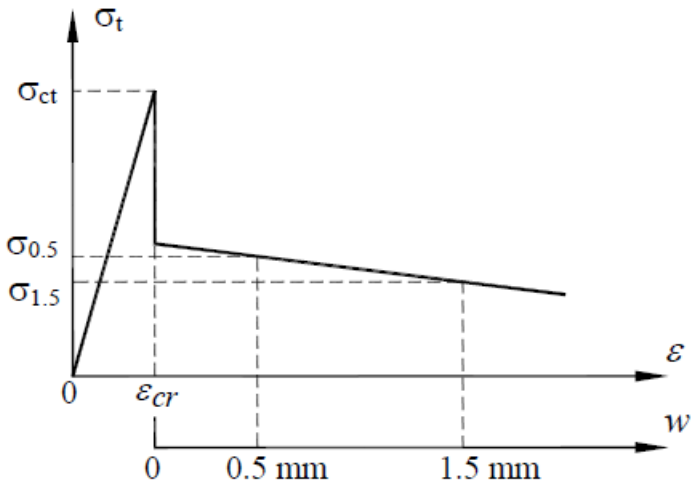


Figure 3.25. Typical stress versus strain and stress versus crack opening displacement for the steel-fiber reinforced concrete in tension (Voo and Foster 2003).

The strength of the concrete matrix is determined by the formula:

$$\sigma_t = \sigma_{ct} e^{-cw} \tag{3.14}$$

where σ_{ct} is the tensile strength of the concrete (f_{ct}), w is the crack opening displacement (mm) and c is an attenuation factor (c=15) (Voo and Foster 2003).

To calculate the contribution of steel fibers to the tensile strength of the concrete specimen, a developed variable engagement model was used, and Equation 3.15 was presented:

$$\sigma_f = K_f K_d \alpha_f \rho_f \tau_b \tag{3.15}$$

where K_f is the global orientation factor, K_d is a fiber efficiency factor ($K_d = 1$), $\alpha_f = l_f/d_f$ is the aspect ratio of the fiber (l_f – length of the fiber, d_f – diameter of the fiber), ρ_f is the volumetric ratio of the fiber, τ_b is the bond strength of the fiber in the matrix ($\tau_b = 2.5 f_{ct}$). K_f can be calculated by Equation 3.16:

$$K_f = \frac{1}{\pi}\, tan^{-1}\left[\frac{w}{\alpha_I l_f}\right]\left(1 - \frac{2w}{l_f}\right)^2 \tag{3.16}$$

where α_I is engagement parameter and $\alpha_I = \frac{1}{3.5\,\alpha_f}$.

Therefore, the tensile stress of the steel-fiber concrete is taken as the sum of the contribution of the concrete matrix (Equation 3.14) and the steel fibers (Equation 3.15).

Based on the peak loads measured for each tests slab and using a fiber efficiency K_d (less than 1.0), Equation 3.17 was found as a good solution to provide an estimate of the efficiency factor in Voo and Foster's model:

$$K_d = 1.63\rho_f - 0.85(\rho_f)^2 \tag{3.17}$$

where ρ_f is the steel-fiber volume.

In this study, 35 mm of end-hooked fibers with 0.7 mm diameter were used. Thus, the aspect ratio α_f of steel fibers is 50. The variations of volumetric fiber ratio ρ_f are 0.5% (40 kg/m^3), 1% (80 kg/m^3) and 1.5% (120 kg/m^3). For better notation ρ_f can be conveniently replaced with ν_f in model for the shear bond slip of steel fiber concrete.

Considering the enhancement of tension stiffening at a crack width of 0.1 mm with the respect of steel fiber dosage and parameters above, the proposed contribution of shear stress at the initiation of slip from the steel-fiber in the slab $\tau_{0,sfrc}$ can be expressed by:

$$\tau_{0,sfrc,} = 0.02 * \left(1.16\nu_f\right)\frac{\alpha_f}{50}\, f_{ct} \tag{3.18}$$

Therefore, Equation 3.13 can be related to the steel-fiber dosage in term of the fiber volumetric ratio v_f as below:

$$\tau_{slip} = \tau_{0,plain} + 0.02 * \left(1.16 v_f\right) \frac{\alpha_f}{50} f_{ct} \quad (3.19)$$

From Daniels and Crisinel's research (1993), the shear strength at slip of plain concrete was taken as $\tau_{0,plain}$ = 0.08 N/mm ^{2}. The mechanical interlock parameter was taken as $\delta_m^f = 5\ mm$. The values of τ_{slip} for composite slabs with 0.5%, 1% and 1.5% of steel fiber are calculated by Equation 3.19 and presented in Table 3.3. The tensile strength of the steel-fiber concrete was assumed to be as $f_{ct} = 2.5\ Mpa$ for all slabs modeled.

Table 3.3. τ_{slip} for steel fiber composite slab when using 35 mm hooked-end type with an aspect ratio of 50 and f_{ct}=2.5MPa.

Steel fiber volume/dosage (%)/(kg/m^3)	τ_{slip} ($\tau_{0,plain}$ =0.08 N/mm ^{2})
0.5% (40 kg/m^3)	0.11
1% (80 kg/m^3)	0.14
1.5% (120 kg/m^3)	0.17

4. RESULTS AND DISCUSSIONS

This section presents the numerical results after analyzing the composite slabs using the finite element method. This simulation uses the fundamental laws of materials, loading procedure, and interaction properties which are already discussed in Chapter 3. In this section, first, mesh convergence analyses are performed to obtain the best mesh size to be used in numerical analyses.

Firstly, the parameters of the interaction such as the shear strength at first slip τ_{slip} and the mechanical interlock parameter δ_m^f that are used in the numerical are discussed. These parameters are discussed in Chapter 3 and depend on the type and shape of the profiled sheet. For plain concrete with deep steel trapezoidal sheet, the shear strength at first slip was taken as 0.08 N/mm^2. This value is based on a study by Burnet and Oehlers (2001) using deep trapezoidal steel sheets. The mechanical interlock parameter δ_m^f was based on the size and shape of the relief on the steel sheet. In the present study, the δ_m^f the value corresponding to the embossed ridge width on the steel sheet surface was taken as 5.0 mm.

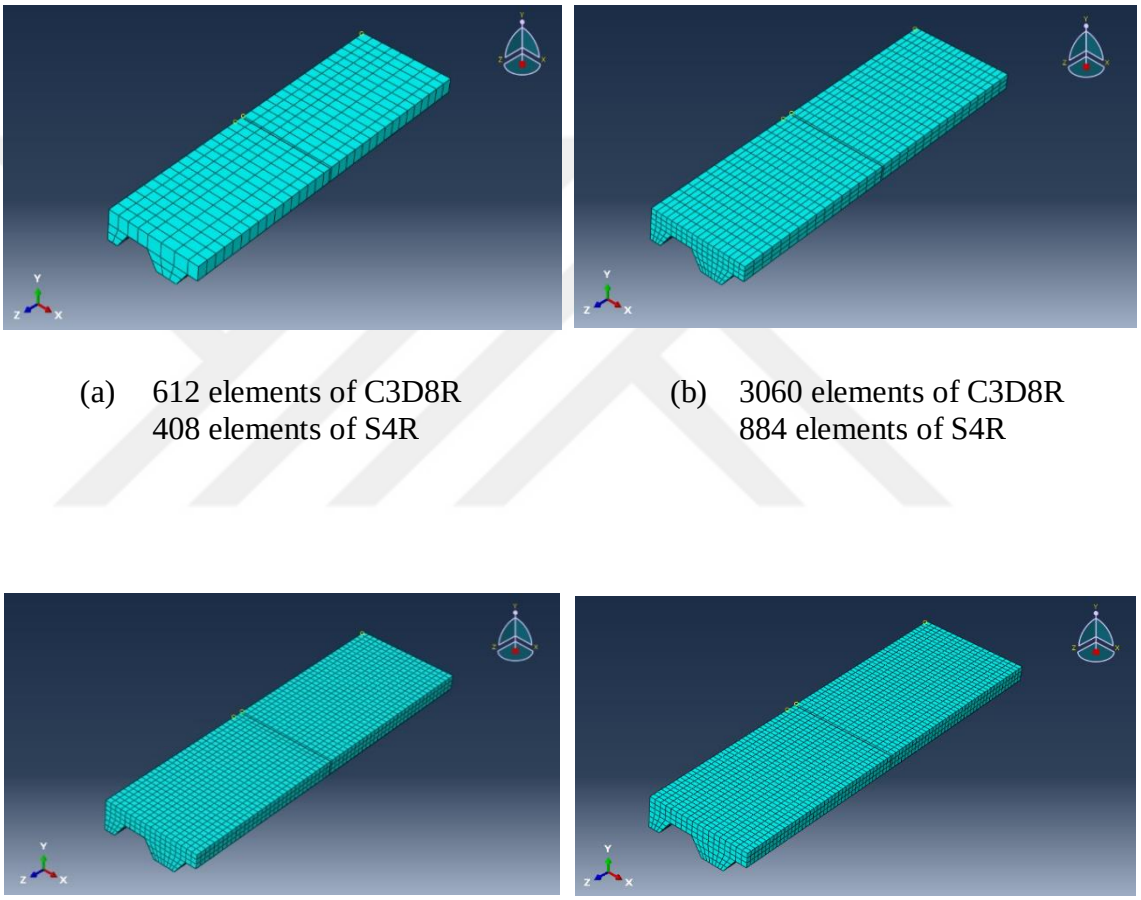
The concrete damaged plasticity (CDP) model, as described in Chapter 3, was used to model the concrete in the composite slabs. All default values were used for the plasticity parameters in the algorithm. Also, using only the elastic model of concrete showed similar good results as the CDP model: the load-carrying capacity of composite slabs is governed by the shear bond capacity between the decking and the concrete. CDP and Elastic models' results in terms of accuracy and speed were compared. Although the results obtained from both models are the same, Elastic model analysis is much faster than CDP model analysis.

4.1. Mesh Convergence

As explained in Chapter 3, the accuracy of the FE model result is dependent on the usage of the optimum mesh size. Therefore, of the mesh convergence analyses are required in order to find accurate mesh sizes. Using coarse meshes promotes fast analyses, but it leads to inaccurate results. In the opposite situation, as the mesh becomes denser, that

means mesh size reduces, there will be a greater demand for computer resources to run this simulation. Therefore, it is required to find an optimum mesh size such that even if mesh size is further reduced, it does not significantly change the results. (ABAQUS Manual 2012.)

In this study, four different mesh sizes are used to perform mesh convergence analyses (Figure 4.1). The number of elements used in each mesh is indicated in the figure.



(a) 612 elements of C3D8R
408 elements of S4R

(b) 3060 elements of C3D8R
884 elements of S4R

(c) 5940 elements of C3D8R
1782 elements of S4R

(d) 7380 elements of C3D8R
2214 elements of S4R

Figure 4.1. Different mesh densities

Effective meshing can be obtained by further partitioning, as indicated in Figure 4.2.

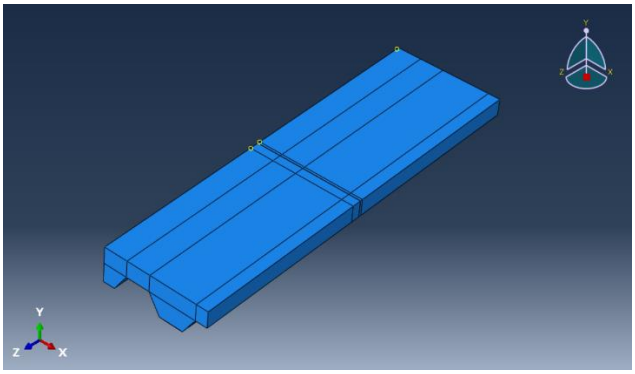
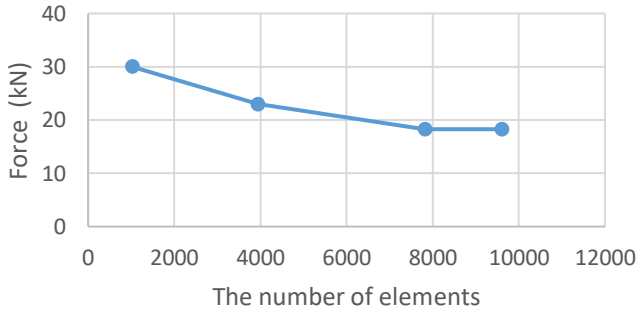
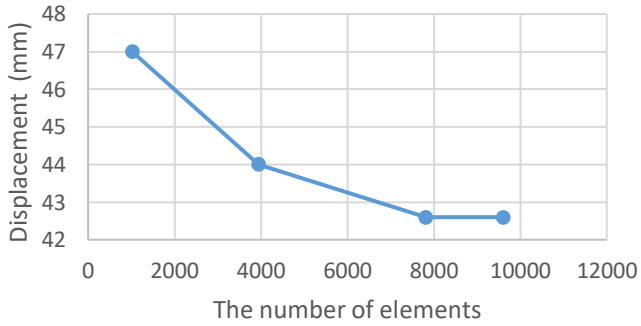


Figure 4.2. Partitions



(a)



(b)

Figure 4.3. Curves of mesh convergence result: (a) force versus the number of elements; (b) displacement versus the number of elements.

According to Figure 4.3 meshing with 7722 elements was found to be accurate mesh size that leads to the converged result for analyzing the composite slabs in this thesis.

4.2 Calibration and comparison of numerical model with the experimental results

In this section, the calibration of numerical models that have been used to investigate the shear-bond behavior of single-span steel-fiber composite slabs with deep trapezoidal decking is discussed. The calibration of the proposed numerical model using experimental results for both plain concrete and steel-fiber concrete was carried out to ensure that the variables and parameters used in the modeling were representatives of the actual response of the concrete composite slab.

In the numerical model, the adhesion bonding and mechanical interlock was represented by defining the cohesive surface interaction with the traction-separation model, which has two calibrating parameters required to be inputted to the program, i.e., the shear strength at first slip τ_{slip} and the mechanical interlock δ_m^f . The friction arising due to the mechanical interlock effect can be simulated at the same time from surface-to-surface interaction using the Coulomb model of friction that has a coefficient of friction parameter, μ between two surfaces in contact.

These model parameters were determined from the test results. The load at which the cohesive bond between the decking and the concrete was broken was easily identified in the laboratory tests, and consequently, the value of shear strength at slip , τ_{slip} was easily calibrated for both the plain concrete and fiber-reinforced concrete composite slabs. The post-slip response of each slab enabled the mechanical interlock parameter, δ_m^f and coefficient of friction, μ to also be calibrated for both the plain and the steel-fiber slabs.

4.2.1 Numerical results for the long composite slabs with plain concrete CS-1, CS-2, CS-3

The load versus mid-span deflection curve predicted by the proposed numerical model is presented and compared with the experimental results in Figure 4.4 for the plain concrete slab. The responses obtained by the numerical analysis are in good agreement with the experimental results.

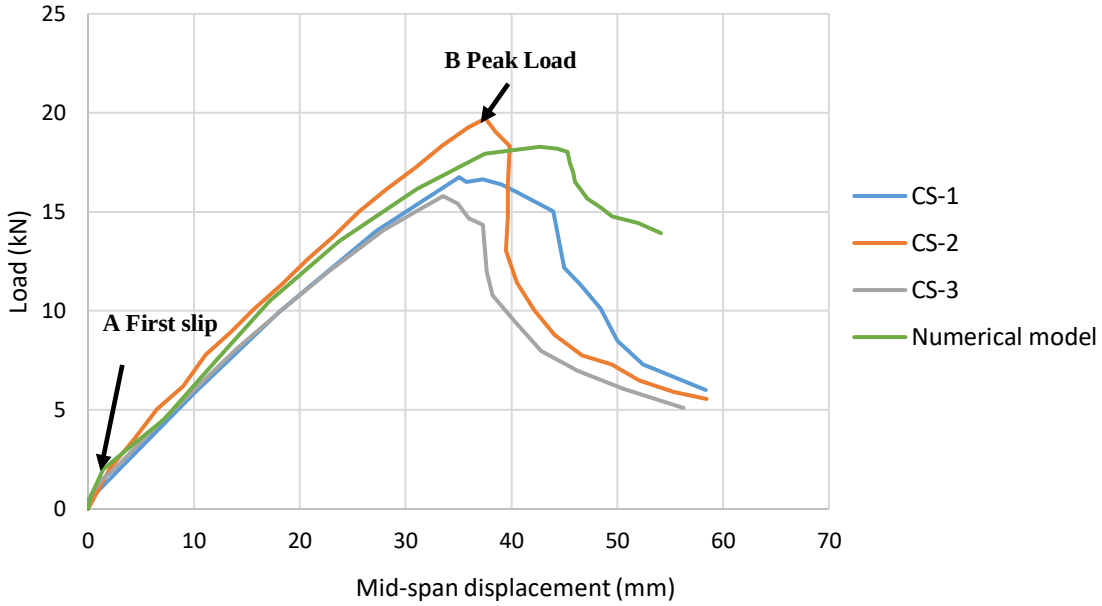


Figure 4.4. Numerical and experimental results of load versus mid-span deflection of slabs CS-1, CS-2, CS-3

The three distinctive regions that represent the behavior of single-span composite slabs are accurately captured by the numerical model. As one can see from figure 4.4, the numerical model accurately captures the elastic behavior (from 0 to point A). At point A, where end slip was initiated as soon as the load reached the slip load denoted, and nonlinear behavior is started at this point. The numerical model predicts the first slip load as 1.99 kN while its average value provided by the experiment is around 1.83 kN. This means that the shear strength parameter at first slip $\tau_{slip} = 0.08\ N/mm^2$ used in the numerical model predicts the slip load very close to one that observed in the laboratory for the plain concrete specimens. The frictional interaction that becomes active when the mechanical interlock interaction starts to engage was dormant during the elastic behavior of cohesive surface interaction but becomes active as soon as the adhesion bond begins to degrade (beyond τ_{slip}) and this gives rise to the longitudinal shear stress at the steel-concrete interface.

The post-slip response of each slab enabled the mechanical interlock parameter, δ_m^f and coefficient of friction, μ to also be calibrated for both the plain and the steel-fiber slabs. In the numerical model, the mechanical interlock parameter , $\delta_m^f = 5mm$ and the

frictional interaction parameter, coefficient of friction $,\mu = 0.6$ used in the numerical behavior to predict post slip response of the composite slab that is based on the size and shape of the embossment on the steel sheeting. As the load progressed beyond the first slip load from point **A to B,** the slope of the load-displacement curve reduced significantly due to induce of damage that causes nonlinear behavior of the slab. The predicted peak load by the proposed numerical model was found to be 18.28 kN, while the averaged value of the peak load obtained from the experiment was recorded as 17.42 kN. A good agreement between the predicted and measured peak loads is achieved with a reasonable difference of 4.9%.

Once the calibration of the model's parameters is completed by identifying the value of all parameters for the plain concrete composite slabs, the prediction capability of the proposed numerical model is validated by simulating load versus displacement curves obtained underneath of the loading point (Figure 4.5) and predicting the magnitude of the slip between the concrete and the decking at the ends of the specimen (Figure 4.6).

Figure 4.5 presents load versus displacement curves obtained from both experimental and numerical studies, and one can see a good agreement between each result.

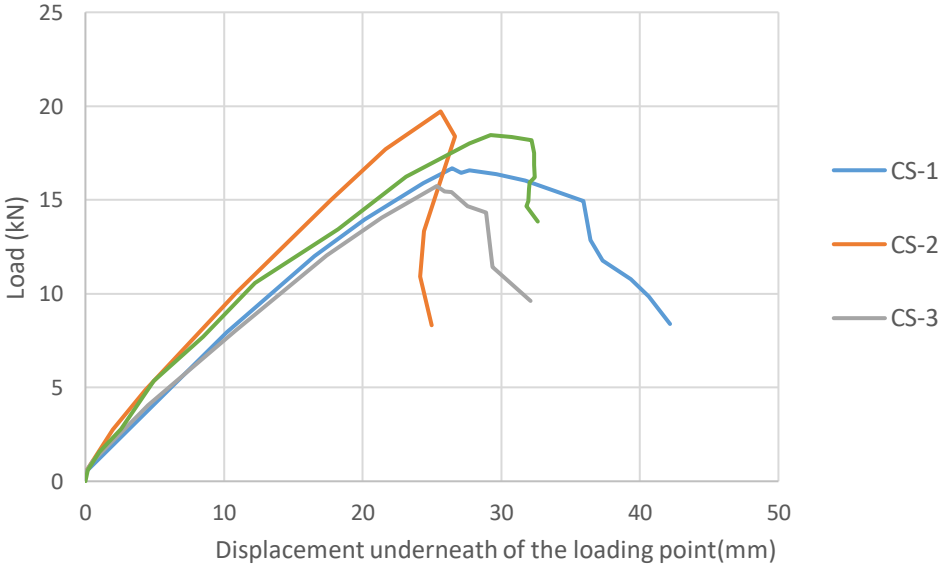


Figure 4.5. Numerical and experimental results of load versus displacement obtained underneath of the loading point of slabs CS-1, CS-2, CS-3

Figure 4.6 shows the comparison of the end-slips obtained by the numerical model and the end slips measured in the experiment. The magnitude of the end slip is found by measuring the relative displacement between the nodes of the steel sheet elements at the member ends and the corresponding nodes of the concrete slab elements. The numerical model predicts the end slip and respective load as 2.5 mm and 18.28 kN, while the average values of these quantities measured from experiments were given as 2.7 mm and 17.42 kN, respectively.

The numerical model results also showed that the slab exhibited ductile-brittle behavior prior to complete failure that is similar to the behavior observed in the experimental studies.

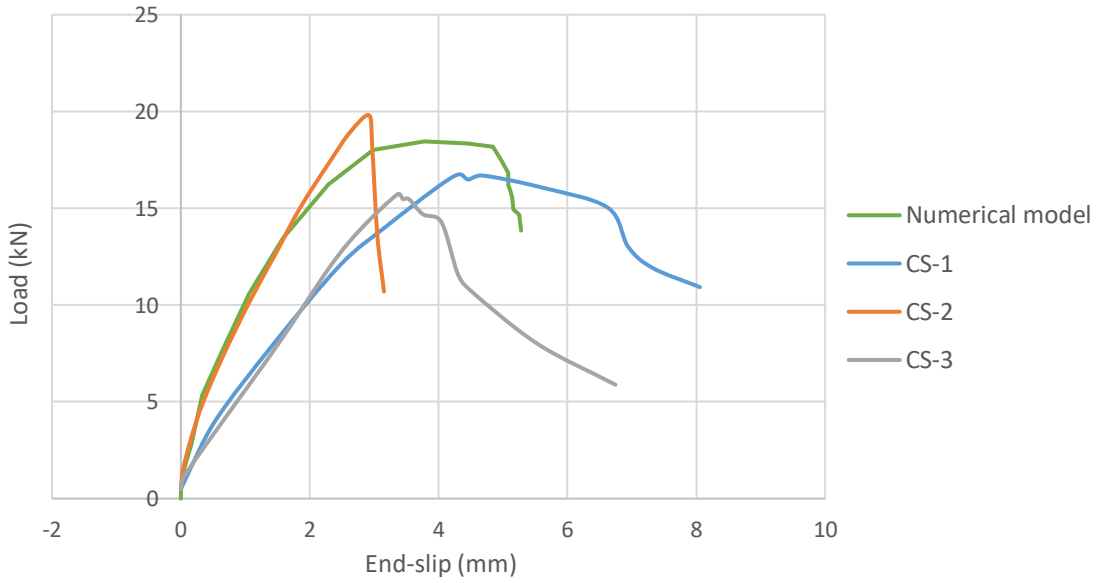


Figure 4.6. Numerical and experimental results of load versus end-slip of long slabs CS-1, CS-2, CS-3.

4.2.2 Numerical results for the short composite slabs CS-5, CS-6.

In this section, the numerical model is used to predict the response of the short slabs **CS-5, CS-6. The results obtained from these numerical analyses are presented in** Figure 4.7. As one can notice that the load versus mid-span deflection curve obtained from numerical model is in good agreement with those curves provided by experiments.

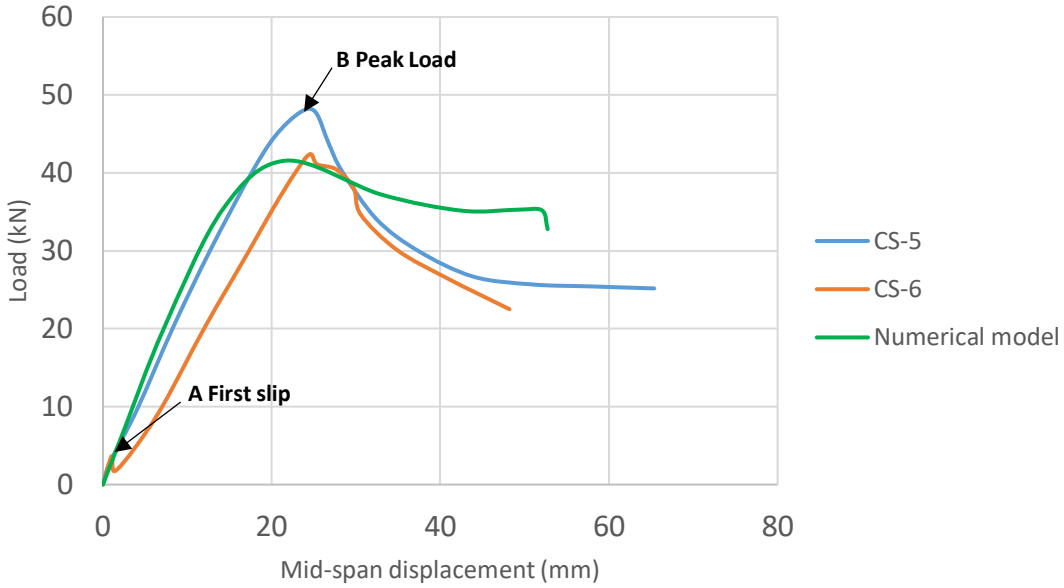


Figure 4.7. Numerical and experimental results of load versus mid-span deflection of short slabs CS-5, CS-6

Three main regions can characterize the complete response of the slab during its loading up to failure. The first one is the elastic zone (from 0 to point A), where the slab does not have residual damages and shows linear behavior. The first slip occurs at the end of this zone, and nonlinear behavior is started at point A. The numerical model predicts the first slip load for the short slab as 3.33 kN, while its value from the experiment is 3.14kN. The results confirm that the shear strength parameter at the first slip used in the numerical model for the short slab predicts the slip load very close to one observed in the laboratory for the short slabs with plain concrete. After point A as soon as the adhesion bond ends, the frictional interaction becomes active because the mechanical interlock interaction starts to engage. The process between points A and B shows how the longitudinal shear stress at the steel-concrete interface rises.

Considering the size, the shape of the embossment on the steel sheeting, and the calibration of these values in the numerical model, the mechanical interlock parameter, $\delta_m^f = 5mm$, and coefficient of friction, $\mu = 0.6$ are used. The average peak load obtained from the experiment was counted as 45.09 kN, while the predicted load by the proposed numerical model was 42.56 kN. It means that results are in good agreement.

Comparison of load versus displacement underneath of the loading point curves is depicted in Figure 4.8.

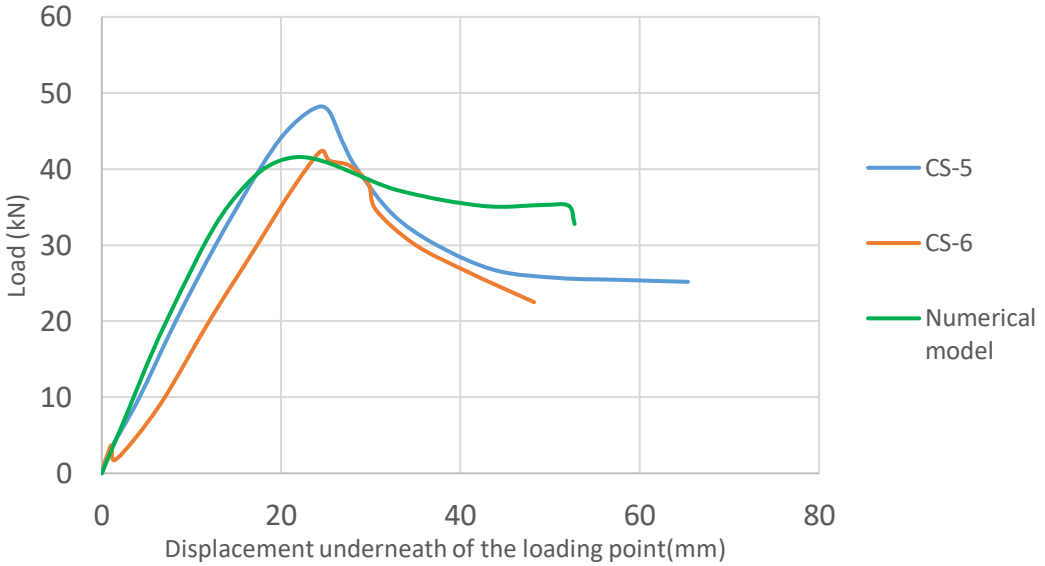


Figure 4.8. Numerical and experimental results of load versus displacement underneath of the loading point of short slabs CS-5, CS-6.

Also, there is a good agreement between experiment tests and numerical results in load versus end-slip curves (Figure 4.9). The numerical model predicts the end slip and respective load as 4 mm and 42.56 kN, while the average values of these quantities measured from experiments were given as 4.36 mm and 45.09 kN, respectively. The magnitude of the end slip is found by measuring the relative displacement between the nodes of the steel sheet elements at the member ends and the corresponding nodes of the concrete slab elements

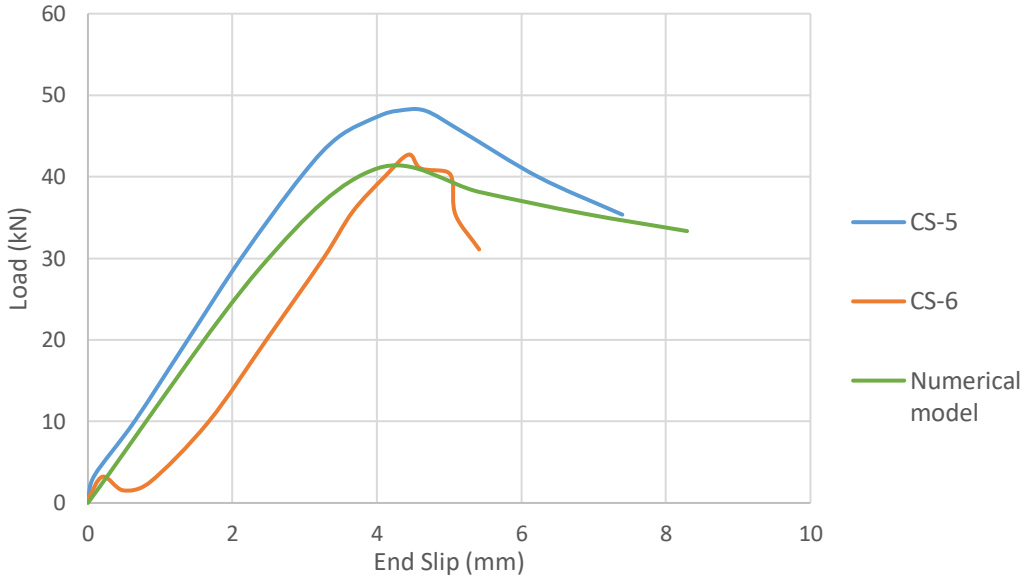


Figure 4.9. Numerical and experimental results of load versus end-slip of short slabs CS-5, CS-6.

4.2.3 Numerical result for the long composite slab CS-7 with 0.5% steel fiber

In this section, the numerical model is used to investigate the effect of various amounts of steel fiber content on the shear bond strength of the long slabs. Figure 4.10 compares the load versus mid-span deflection curves obtained from the experimental slab with 0.5% of steel fiber and the numerical model.

By the Variable Engagement Model developed by Voo and Foster (2003) and Equation 3.19 (details were presented in Chapter 3), in the numerical model of the composite slab with 0.5% steel fiber concrete, the shear strength τ_{slip} should be taken as 0.11 N/mm ^{2}.

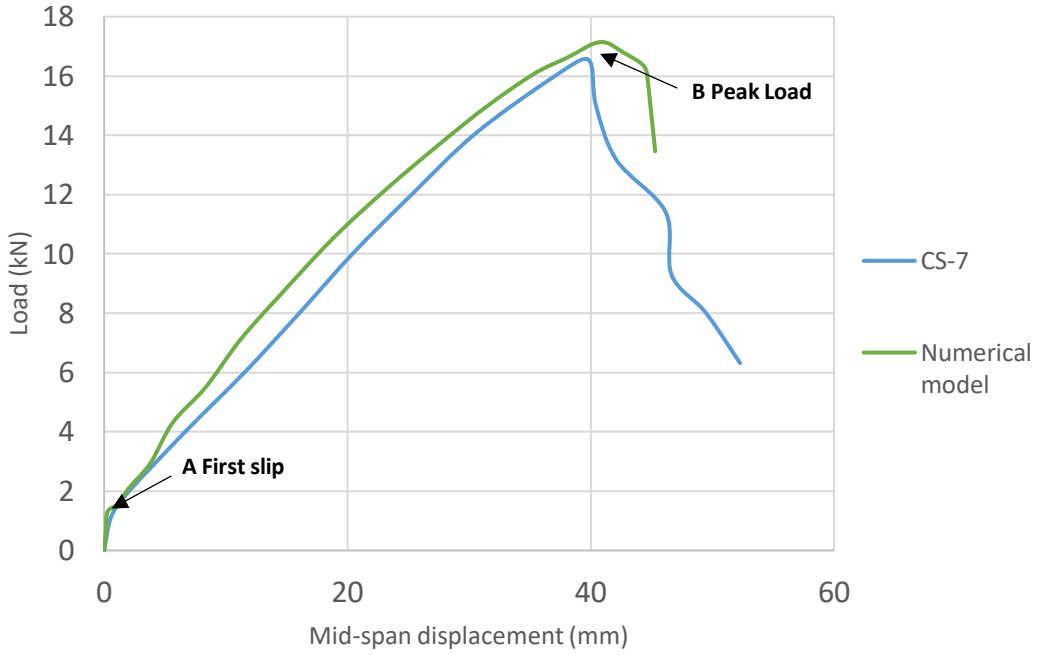


Figure 4.10. Numerical and experimental result of load versus mid-span deflection of long slab CS-7 and numerical model (0.5% steel fiber).

From the result obtained, three phases can be observed. The first phase was in the low load region (from 0 to A point). In this phase, the slabs behaved elastically. At the end of this phase, the first slip occurs what means that the adhesion bond begins to degrade (beyond τ_{slip}). The numerical model predicts the first slip load as 1.55 kN while its average value provided by the experiment is around 1.76 kN.

The second phase between points A and B was after the first slip appeared. Here irreversible damages have occurred because the mechanical interlocking interaction begins to act, and the frictional interaction becomes active.

The third phase happened after the occurrence of the maximum end-slip between the decking and the concrete. The overall stiffness of the slab reduced significantly as the load progressed towards the failure load (after the B point). The numerical model predicts the maximum failure load as 17.14 kN while its value provided by experiment is around 16.45 kN. It means that the numerical model predicts the maximum failure load accurately with a 3.5% difference as compared to the experimental value. It showed good agreement between results.

Since all the composite slabs in this study used the same type of steel decking, the same mechanical interlock parameter ($\delta_m^f = 5mm$) and the same frictional interaction parameter ($\mu = 0.6$) are used in the numerical behavior to predict the post slip response of the composite slab.

Figure 4.11 shows the comparison of displacement underneath of the loading point obtained numerically and measured in the experiment for the slab CS-7.

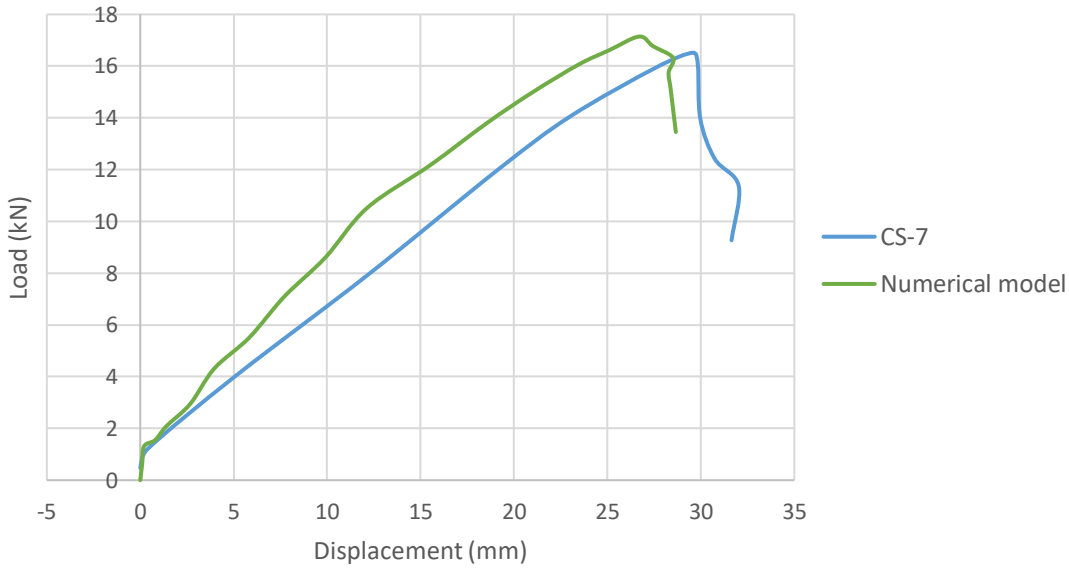


Figure 4.11. Numerical and experimental result of load versus displacement obtained underneath of the loading point of long slab CS-7

By adding 0.5% of steel fiber, as a result, the end slip increased as compared to the results of composite slabs with plain concrete. It is seen from Figure 4.12 in comparison with Figure 4.6. The average values of the end slip and the respective load was given as 3.77 mm and 16.45 kN, respectively, while the numerical model predicts the end slip and respective load as 3.3 mm and 17.14 kN.

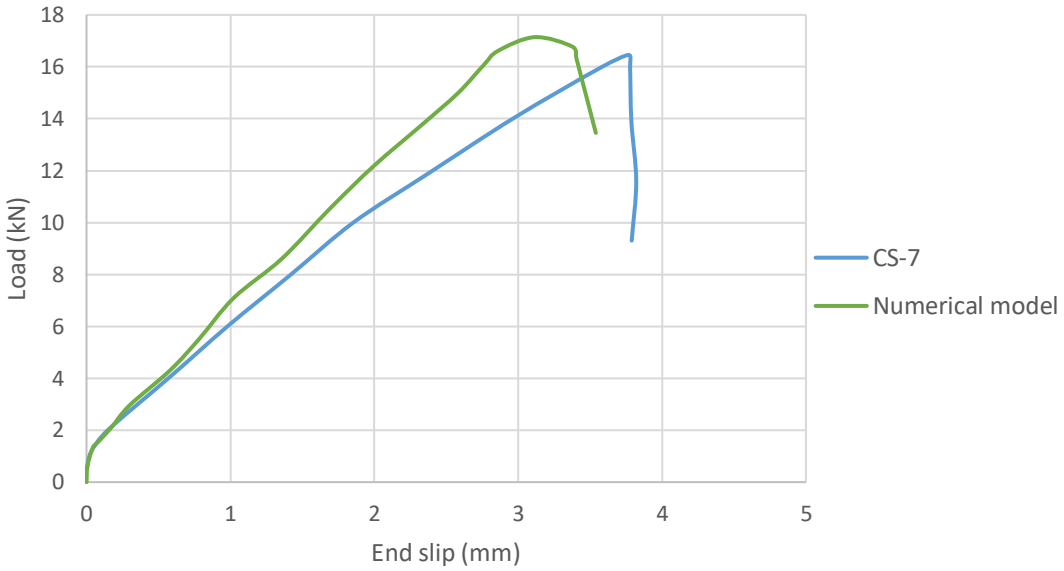


Figure 4.12. Numerical and experimental results of load versus end-slip of long slab CS-7 with 0.5% steel fiber.

4.2.4 Numerical result for the long composite slab CS-8 with 1% steel fiber

The load versus mid-span displacement predicted by the numerical model with 1% steel fiber in comparison with experiment result is shown in Figure 4.13.

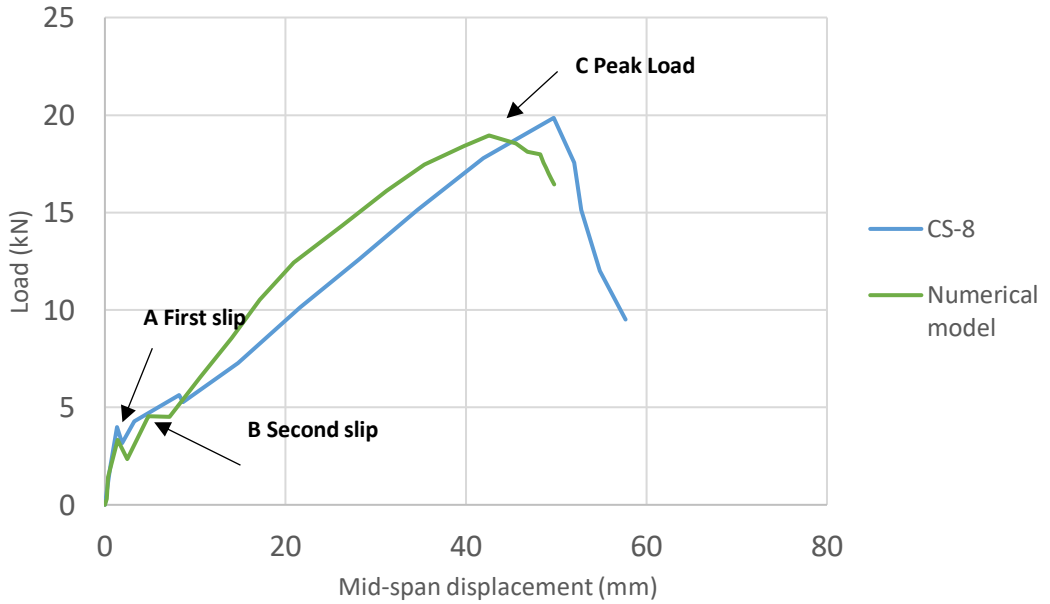


Figure 4.13. Numerical and experimental result of load versus mid-span displacement of long slab CS-8 (1% steel fiber).

According to Voo and Foster's graphs and formulas for calculating the shear strength τ_{slip} for the steel fiber concrete (described in Chapter 3) and Daniels and Crisinel's research about the first slip of composite slabs with plain concrete, the shear stress for simulating CS-8 was taken as 0.14 N/mm^2 (Table 3.3).

As seen, the first slip formed in point A, when the maximum load of the elastic zone was 3.52 kN. The load at the first slip of the experiment was 3.89 kN, which is 9.5% of the difference with the numerical model's result. In the experiment, the second slip (point B) occurred when the load was 5.62 kN, while the load of the numerical model was 4.53 kN. After slips, the load continued to increase with reduced stiffness beyond the slip load. All slabs exhibited high deformability as the load approached the peak value (non-linear behavior and effect of mechanical interlock). The slab CS-8 with steel fiber dosage of 80 kg/m3 (v_f = 1%) had a peak load of 18.94 kN in the numerical model and 19.85 kN in the experiment. Displacement in peak load at numerical model was 42.6 mm, while in the test, it was 49.75 mm. In comparisons of experimental and numerical results, a difference within 20 percent is considered acceptable. The difference between displacements obtained is 14.37%.

Below in the Figure 4.14 load versus displacement obtained underneath of the loading point of long slab CS-8 is presented and compared with the experiment.

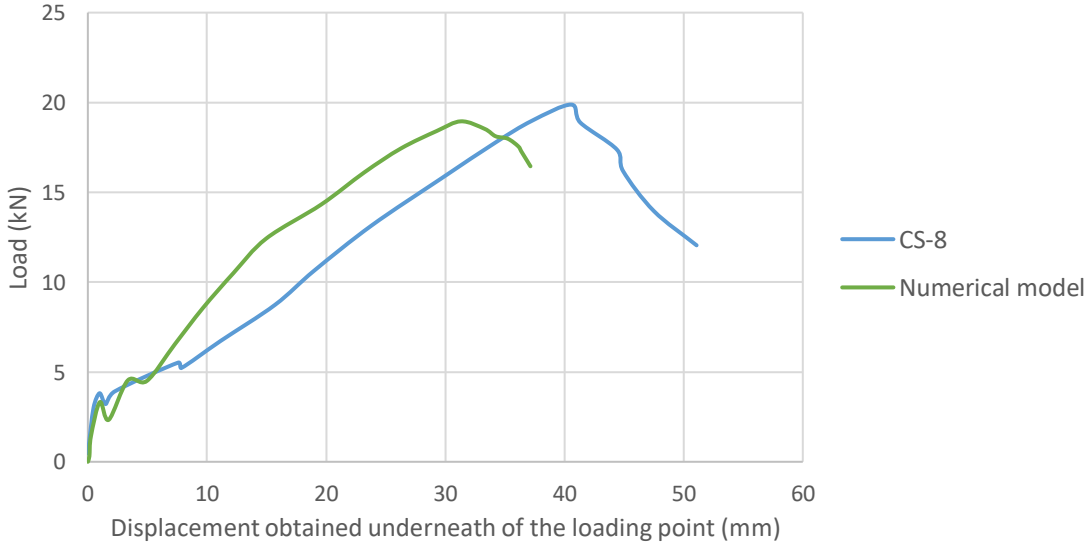


Figure 4.14. Numerical and experimental result of load versus displacement obtained underneath of the loading point of long slab CS-8 (1% steel fiber).

Curves of load versus end-slip (Figure 4.15) proves that the slip initiation load and end-slip displacement are increased by increasing the steel-fiber content. This can be seen from the comparison of Figures 4.15 and 4.6. The numerical model of CS-8 predicts the end slip and respective load as 4.52 mm and 18.94 kN, while the average values of these quantities measured from the experiment were given as 5.1 mm and 19.85 kN, respectively.

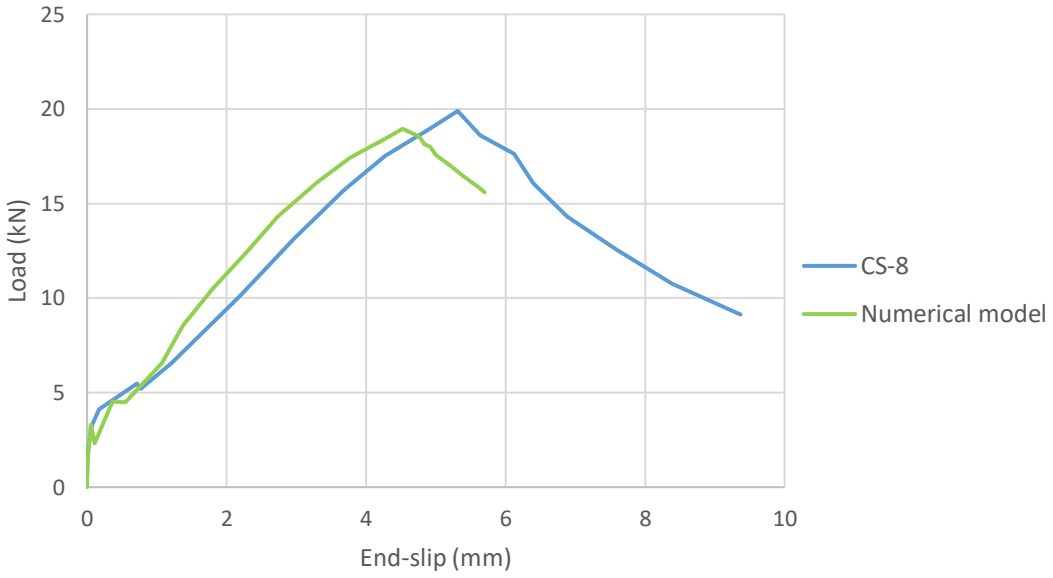


Figure 4.15. Numerical and experimental result of load versus end-slip of long slab CS-8 (1% steel fiber).

Moreover, it can be seen from previous tests that by adding the steel fibers to the slab, the load-carrying capacity is increased compared to the plain concrete slab.

4.2.5. Numerical result for the long composite slab CS-9 with 1.5% steel fiber

The last slab in the experiment was a long slab with 1.5% steel fiber. In this case, the appearance of the first slip was taken when the value of shear stress was 0.17 N/mm^2. This value was calculated by Equation 3.19 and presented in Table 3.3 with detail explanation in Chapter 3. Curves of load versus mid-span displacement for CS-9 are depicted in Figure 4.16.

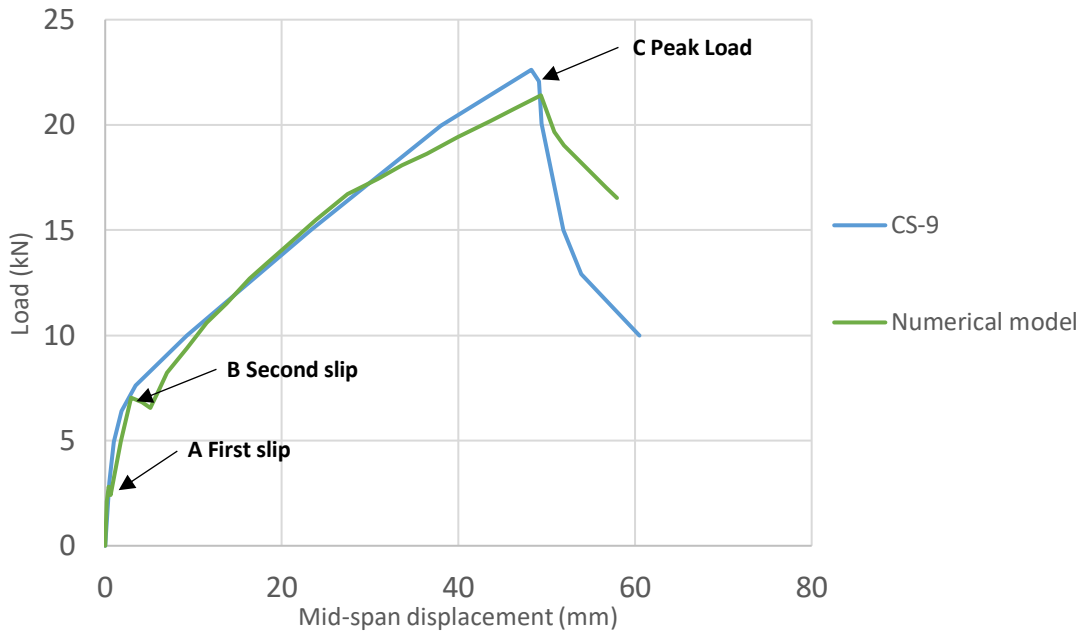


Figure 4.16. Numerical and experimental result of load versus mid-span displacement of long slab CS-9 (1.5% steel fiber).

Figure 4.16 shows that the slab with 1.5% steel fiber had high stiffness in the elastic zone as in the experiment test and a numerical model. In the curve obtained from the numerical model, the first slip occurred when the load was 2.5 kN (point A). The second slip occurred when the load dropped slightly at the value of 7.04 kN (point B). In the graph obtained from the experiment, it is not obvious at what value the slippage occurred. But when the load reached 6.8 kN, the elastic zone ended. This fact gives the right to assert that before getting this value, two slips have already occurred in the experiment. As mentioned above, after the onset of sliding, the adhesive bond is destroyed, and the frictional behavior is activated due to the start of mechanical interlock interaction. The predicted peak load by the proposed numerical model was as 21.4 kN, while the averaged value of the peak load obtained from the experiment was found as 22.16 kN.

Figure 4.17 represents the comparison of curves of load versus displacement obtained underneath the loading point from the experiment and numerical model. A good agreement can be seen from these results.

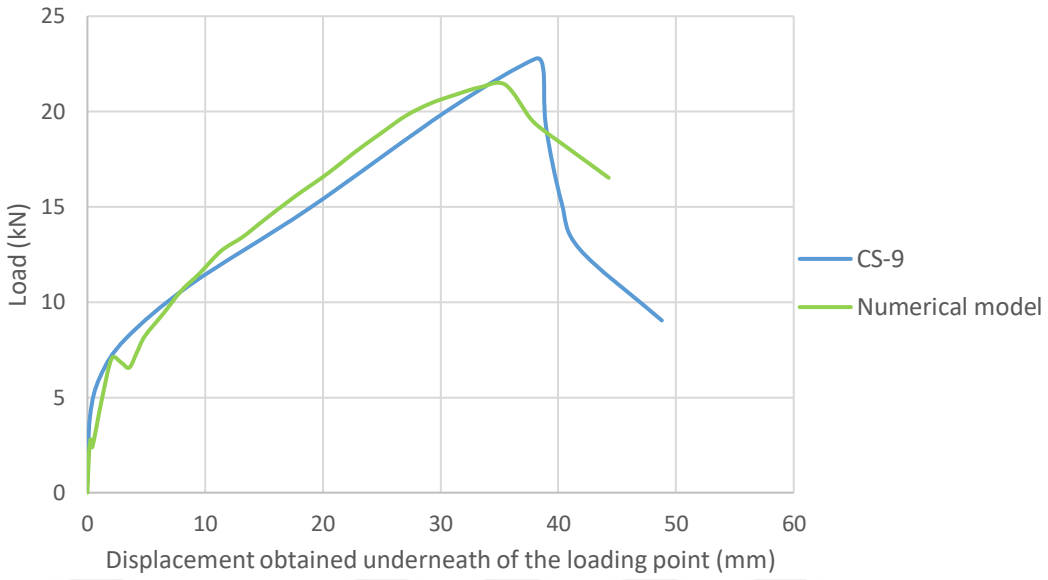


Figure 4.17. Numerical and experimental result of load versus displacement obtained underneath of the loading point of long slab CS-9 (1.5% steel fiber).

Figure 4.18 represents the load versus end-slip graphics obtained from the test and the numerical model. From the results, it becomes apparent that the 1.5% steel fiber content increased the load-bearing capacity and the end slip of the composite slab compared to composite slabs with plain concrete.

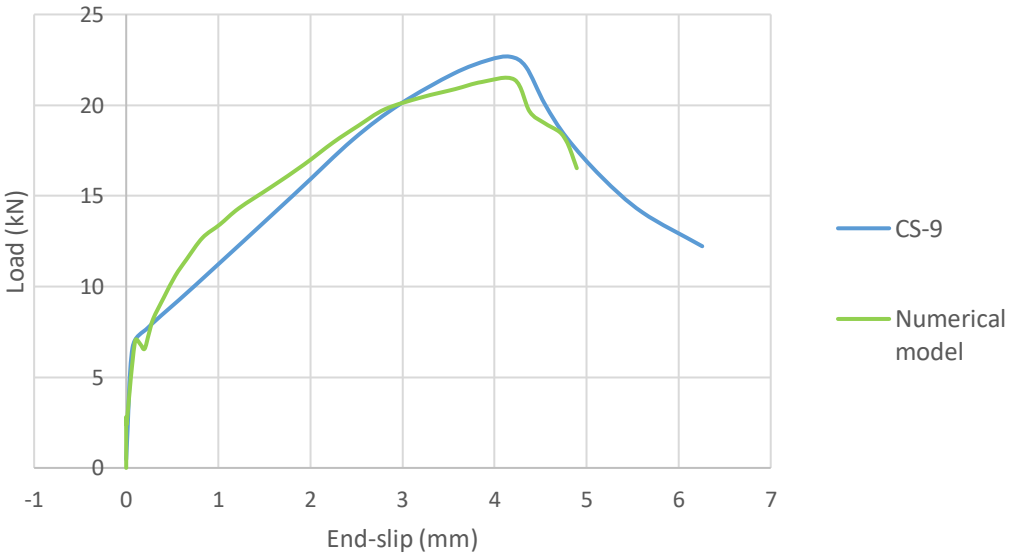


Figure 4.18. Numerical and experimental results of load versus end-slip of long slab CS-9 (1.5% steel fiber).

4.3. Comparison of the results obtained from laboratory tests, m-k method, Partial connection method and numerical model.

In this chapter, results for long-span slabs from the thesis by Başsürücü (2013) were compared with numerical model results. The confirmation of results obtained from simulations gives a realistic simulation of the non-linear behavior of composite slabs. The difference in the values as a percentage is presented in Table 4.1. The result from numerical models was found to be within acceptable range with laboratory tests, m-k, and partial connection methods.

Table 4.1. The comparison of the results obtained from laboratory tests, m-k method, partial connection method, and numerical model.

(a)

Name of specimen	**m (N/mm^2)**	**k (N/mm^2)**	**τ_u (N/mm^2)**	**m-k method W (kN)**	**τ method W (kN)**	**Numerical model W (kN)**	**m-k Difference (%)**	**τ Difference (%)**
CS-1	107.8	-0.048	0.0629	9.23	9.62	9.17	-0.65	-4.67
CS-2	107.8	-0.048	0.0629					
CS-3	107.8	-0.048	0.0629					

(b)

Name of specimen	**Experiment W (kN)**	**Numerical model W (kN)**	**Experiment Hata (%)**
CS-1	9.21	9.17	-0.43
CS-2	9.54		-3.87
CS-3	8.88		-3.26

Differences less than 10% are acceptable and mean a good agreement.

5. CONCLUSION

As it is known that there are no analytical formulas for calculating the strength of composite slabs; therefore, the main aim of this thesis was to simulate the most realistic behavior of composite slabs. The ability to simulate the realistic behavior will allow all manufacturing companies producing different steel decks not to conduct many full-scale experiments for each type of deck. The successful simulation will reduce material costs, time, labor, and simultaneously, it will provide results close to reality. In this study, simulations of composite slabs with plain concrete and concrete with different dosages of steel fiber (0.5%, 1%, and 1.5%) were conducted using the ABAQUS/Explicit software. The greatest attention was paid towards modeling the relationship between steel deck and concrete. The behavior between the steel deck and concrete during loading was divided into two stages: before the first slip occurs (chemical bond) and after the first slip occurs (mechanical and frictional behavior). The following conclusions are drawn from the study:

- The successful composite slab simulation was performed that demonstrated the cohesive and frictional behavior between the steel deck and concrete. It can further be used to understand better the bond between concrete and the steel deck and predict the ultimate capacity of such structures without much cost. As seen from the results, the obtained model successfully simulates composite slabs under static loads.

- Different ways of determining the non-linearity of materials have been studied. Firstly, the CDP model was chosen to model concrete, but later the linear model was used. It happened because the failure in all experiments happened because of longitudinal stress. Also, in the Finite Element Model, the failure is obtained by exceeding the longitudinal shear strength. As a result of the comparisons between the CDP model and the linear model with failure in longitudinal shear strength, it turned out that the results are almost the same, but speed is faster in the linear model. Therefore, using CDP was not the most efficient because it made the duration of analysis slower and gave similar values.

- The proposed model relating the shear bond at first slip to the tensile stress in the steel-fiber concrete at 0.1 mm crack width was found to be a viable means for predicting the initiation of first slip in the steel-fiber reinforced concrete composite slabs. The model could be used to predict the slip load with various other steel fiber dosages and for different deck profiles provided that the shear bond at the slip and the post-slip response are calibrated from standard push tests.

- Good agreement has been demonstrated between the numerical results and the measured response of single-span slabs tested to failure and reported in Chapter 4. The load-deflection responses and the end-slips were closely monitored.

- The laboratory experiments and the numerical modeling have demonstrated an increase in the slip initiation load, mid-span, and end-slip displacements by increasing the steel-fiber content in concrete. This is clearly seen in comparing the results of composite slabs with plain concrete and concrete with different volumes of steel fiber.

- The values of the load at the steel-concrete interface predicted by the numerical model were in reasonable agreement with the loads from experiment tests, evaluation from the partial interaction method, and the shear force evaluated by m-k method.

REFERENCES

ABAQUS Analysis User's Manual. 2012. *K. Hibbit, Sorensen, Dassault Systems, Simulia Corp.*

Abas, F.Z.M. 2014. *Strength of fiber reinforced concrete slabs with deep trapezoidal profiled steel decking. PhD thesis*. The University of New South Wales.

Abbas, A. and Mohsin, S.S., 2010. *Numerical modeling of fiber-reinforced concrete.* International Conference for Computing in Civil and Building Engineering (ICCCBE).

Abdullah, R., Easterling, W. Samuel. 2008. *New evaluation and modeling procedure for horizontal shear bond in composite slabs. J of Constructional Steel Research*, 65:891–9.

Asahaad, M. 2018. *Bond behavior of CFRP and flexible adhesive in masonry walls experimental and numerical research. Master's thesis.*

Attarde, S. 2014. *Nonlinear finite element analysis of profiled steel deck composite slab system under monotonic loading. Master's thesis.*

Bastian, E. Rapp. 2017. *Microfluidics: Modeling, Mechanics and Mathematics. Book. Journal Elsevier.*

Başsürücü, M. 2013. *Experimental determination of longitudinal shear capacity of composite slab system. Master's thesis.* Mustafa Kemal University. Hatay.

Chaudhari, S.V. and Chakrabarti, M.A., 2012. *Modeling of concrete for nonlinear analysis using finite element code ABAQUS. International Journal of Computer Application (0975-8887),* Vol. 44(7).

Chen, S. and Shi, X., 2011. *Shear bond mechanism of composite slabs - A universal FE approach. J of Constructional Steel Research 67(10)* pp: 1475-1484.

Cifuentes H, Medina F., 2013. *Experimental study on shear bond behavior of composite slabs according to Eurocode 4. J of Constructional Steel Research,* 82:99–110.

Crisinel, M. and Marimon, F., 2004. *A new simplified method for the design of composite slabs. J of Constructional Steel Research* 60(3–5): 481-491.

Daniels, B. J. and Crisinel, M., 1993. *Composite Slab Behavior and Strength Analysis. Part I: Calculation Procedure. J of Structural Engineering* 119(1), pp: 16-35.

Daniels, B. J. and Crisinel, M., 1993. *Composite Slab Behavior and Strength Analysis. Part II: Comparisons with Test Results and Parametric Analysis. J of Structural Engineering* 119(1), pp: 36-49.

Eurocode 4, EN1994-1-1:2005. 2005. *Design of Composite Steel and Concrete Structures - Part 1-1:* General Rules and Rules for Buildings (including Irish National Annex).

Ferrer, M., Marimon, F., Crisinel, M., 2006. *Designing cold-formed steel sheets for composite slabs: An experimentally validated FEM approach to slip failure mechanics. Thin-Walled Structures* 44(12), pp: 1261-1271.

Foster, S.J., 2009. *The application of steel-fibers as concrete reinforcement in Australia: from material to structure. Materials and Structures* 42(9), pp: 1209-1220.

Gholamhoseini A, Gilbert RI, Bradford MA, Chang ZT., 2014. *Longitudinal shear stress and bond-slip relationships in composite concrete slabs. Engineering Structures. Elsevier*, 69: 37–48.

Jason, L., Huerta, A., Pijaudier-Cabot, G., Ghavamian, S. 2004. *An elastic plastic damage formulation for concrete: application to elementary tests and comparison with an isotropic damage model.* Comput. Methods Appl. Mech. Eng. 195(52): 7077–7092.

Nethercot, D.A., 2003. *Composite Construction. Book. Spon Press.*

Oehlers, D. J., Bradford, M.A., 1995. *Composite Steel and Concrete Structural Members: Fundamental Behavior. Pergamon Press.*

Özcan, D. M., Bayraktar, A., Şahin, A., Haktanir, T., Tùrker, T., 2009. *Experimental and finite element analysis on the steel fiber-reinforced concrete (SFRC) beams ultimate behavior. Construction and Building Materials* 23(2), pp: 1064-1077.

Patrick, M. and Bridge, R. Q., 1994. *Partial shear connection design of composite slabs. Engineering Structures* 16(5), pp: 348-362.

Qureshi, J., 2010. *Finite element modeling of a push test with trapezoidal metal decking.* The Institution of Structural Engineers Young Researcher's conference (YRC2010). London, United Kingdom.

Ríos, J.D., Cifuentes, H., Martínez-De La Concha, A., Medina-Reguera, F., 2016. *Numerical modeling of the shear-bond behavior of composite slabs in four and six-point bending tests. Engineering Structures, Elsevier,* pp: 0141-0296.

Schuster, R. M. and Ling, W. C., 1980. *Mechanical interlocking capacity of composite slabs. Fifth international specialty conference on cold-formed steel structures* (1980: November 18-19; St. Louis, Missouri), Missouri S&T (formerly the University of Missouri - Rolla).

Sun, J. S., Lee, K. H., Lee, H. P., 2000. *Comparison of implicit and explicit finite element methods for dynamic problems. Journal of Materials Processing Technology 105*(1–2), pp: 110-118.

Toussi, O.M., Sarir, P., 2016. *Finite Element Analysis of Composite Deck Slab Using Perfobond Rib as Shear Connection System under Vertical Loading. J of Engineering Research and Applications*, pp.72-74.

Tremblay, R., Rogers, C. A., Gignac, P., Degrangel, G., 2002. *Variables Affecting the Shear-bond Resistance of Composite Floor Deck Systems.* Sixteenth International Specialty Conference on Cold-Formed Steel Structures Orlando, Florida USA, pp: 663-676.

Vainiūnas, P., Valivonis, J., Marčiukaitis, G., Jonaitis, B., 2006. *Analysis of longitudinal shear behavior for composite steel and concrete slabs. Journal of Constructional Steel Research* 62(12), pp: 1264-1269.

Vakil, M.D., 2017. *Investigations on flexural capacity of steel concrete composite deck with diverse bond patterns. PhD thesis.* Gujarat Technological University.

Veljkovic, M., 1996. *Behavior and Resistance of Composite Slabs - Experiments and Finite Element Analysis.* Lulea University of Technology.

Watts, T., Kayvani, K., Kucyper, A., 2013. *Application of explicit finite element analysis in solving practical structural engineering problems.* From Materials to Structures: Advancement through Innovation. A. S. E. Samali, Taylor & Francis Group, London, pp: 219-224.

Wright, H. D., Evans, H. R., Harding, P. W., 1987. *The Use of Profiled Steel Sheeting in Floor Construction. Journal of Constructional Steel Research (7*), pp: 279-295.